2019

Techno-Economic and Sustainability Study of PV Inverter Controllers in Distribution Networks for Voltage Regulation

Kapil Duwadi
South Dakota State University

TECHNO-ECONOMIC AND SUSTAINABILITY STUDY OF PV INVERTER CONTROLLERS IN DISTRIBUTION NETWORKS FOR VOLTAGE REGULATION

BY

KAPIL DUWADI

A thesis submitted in partial fulfillment of the requirements for the

Master of Science

Major in Electrical Engineering

South Dakota State University

2019

TECHNO-ECONOMIC AND SUSTAINABILITY STUDY OF PV INVERTER CONTROLLERS IN DISTRIBUTION NETWORKS FOR VOLTAGE REGULATION

KAPIL DUWADI

This thesis is approved as a creditable and independent investigation by a candidate for the Master of Science in Electrical Engineering degree and is acceptable for meeting the thesis requirements for this degree. Acceptance of this thesis does not imply that the conclusions reached by the candidates are necessarily the conclusions of the major department.

Timothy M. Hansen, Ph.D.
Thesis Advis Date

Robert Fourney, Ph.D.
Thesis Advisor Date

George Hamer, Ph.D.
Department Head
Electrical Engineering and Computer Science Date

Dean, Graduate School Date

ACKNOWLEDGEMENTS

I would like to express my sincere gratitude towards my thesis advisors Dr. Timothy M. Hansen, Dr. Reinaldo Tonkoski, and Dr. Robert Fourney for their continuous guidance and encouragement. I would like to acknowledge them for providing valuable insight into every step of this work. This work would not be possible without their patience, motivation, and enthusiasm.

Besides my advisors, I would like to thank graduate faculty representative Dr. Dwayne Beck, for his participation and interest in my work.

I am very thankful to Rupak, Ujjwol, Venkat, Fernando for sharing their work and experience with me. I am grateful to my friends Abodh, Aravind, Samitinjaya, Bikram, Romancha, Prateek, Priti, Abhilasha, Andre, Shuva, Avijit, Naren, Rashedul their for support and encouragement.

I would also like to acknowledge Dr. Jessica Ulrich-Schad, Dr. Maaz Gardezi, and Brenton William Thompson for reviewing my Thesis.

Finally, I would like to express my gratitude to my parents, Kamal Prasad Duwadi and Gita Devi Panthi Duwadi, my brother Bikalpa Duwadi for providing me with unfailing support and continuous encouragement throughout my study and research.

CONTENTS

ABBREVIATIONS

ARD	Active-Reactive Droop
ARPM	Active and Reactive Power Management
FRT	Fixed Rate Tariff
HPC	High-Performance Computing
LCPV	Levelized Cost of PV System
LDAPC	Linear Droop based Active Power Curtailment
NSGA	Non-dominated Sorting Genetic Algorithm
OVP	Overvoltage Prevention
PV	Photovoltaic
QDAPC	Quadratic Droop based Active Power Curtailment
QSTS	Quasi Steady State Time Series
RTP	Real Time Pricing
TOU	Time of Use

LIST OF FIGURES

ABSTRACT

TECHNO-ECONOMIC AND SUSTAINABILITY STUDY OF PV INVERTER CONTROLLERS IN DISTRIBUTION NETWORKS FOR VOLTAGE REGULATION

KAPIL DUWADI

2019

Increasing distributed solar installations in low voltage distribution grids tend to increase the feeder voltage. The rise in voltage is only acceptable to a certain limit, and control strategies are required to keep voltage within defined bounds for equipment safety and system reliability. PV inverter control strategies are cost-effective methods to prevent overvoltage. Different inverter control strategies have different impacts on their techno-economic performance, ultimately affecting their sustainability. An evaluation framework for long-term techno-economic and sustainability analysis of overvoltage prevention methods in PV-rich LV networks is proposed to decide suitable control methods by making use of quasi-steady-state time-series (QSTS) software (GridLAB-D). A power network sensitivity-based algorithm is also proposed for preventing numerical oscillation while implementing active and reactive droop-based PV inverter controllers in QSTS (i.e., GridLAB-D). Convergence of the sensitivity-based algorithm is verified using a typical radial distribution feeder for three droop-based PV inverter controllers limiting the error below 0.5%. Techno-economic performance was analyzed by looking into voltage profile, energy generation, and consumption, energy losses, impact on transformer overloading and financial impact on government, utility, and end-users.

Three different sustainability metrics are proposed to quantify these impacts for

inverter-based voltage control strategies. Five different PV inverter control strategies are implemented in a radial distribution feeder and power flow is analyzed for one year in a one-minute resolution to compute and compare the proposed sustainability metrics. The use of reactive power improved sustainability compared to just using active power curtailment. The trade-off of the three objectives was compared using multi-objective optimization for the highest solar irradiance day. Results showed that economic and environmental sustainability are positively correlated, and both are negatively correlated with social sustainability, indicating a required trade-off for voltage control strategies. The proposed framework can aid utilities to decide the most effective control and pricing methods, and whether investments in overvoltage prevention infrastructure can be justified under a high penetration scenario.

Lastly, a distribution optimal power flow is formulated to determine the locational marginal price for distribution grid ancillary services such as active power curtailment and reactive power absorption. Additionally, a Monte Carlo based PV hosting capacity analysis is performed in Taxonomy Feeder for highest irradiance and low load day using High-Performance Computing. Results showed that overvoltage becomes an issue even at 10% penetration level.

CHAPTER 1 INTRODUCTION

1.1 Background and Literature Review

Currently, the total U.S solar installation is 58.3 gigawatts (GW), enough to power 11 million American homes, and is expected to double by the year 2023 [1]. Improving economic viability, incentives, state renewable portfolio standards are making distributed photovoltaic (PV) systems more common [2], [3]. Even though the overall contribution of distributed PV generation to the electricity remains relatively low —less than 0.4% in the United States, around 32% of the total solar energy generation came from the distributed PV in 2018, out of which 58% came from the residential sectors [4] as shown in Fig. 1.1. Eight utilities located across the United States have observed a tenfold increase in the

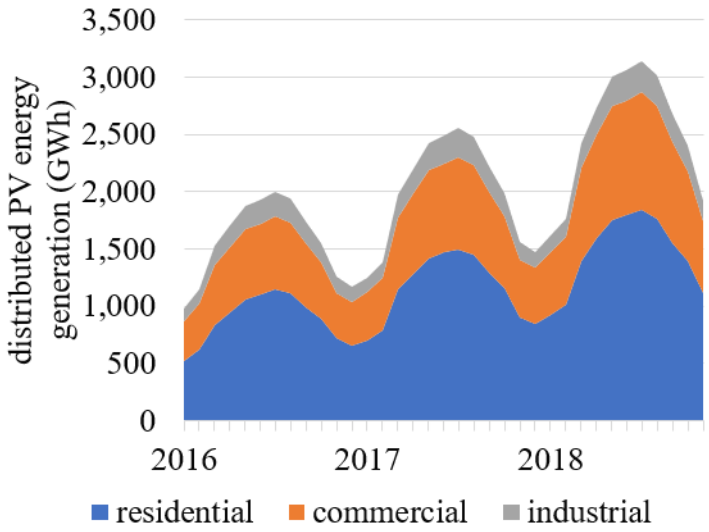

Figure 1.1. Share of residential, commercial and industrial sector in distributed solar energy generation from 2016 to 2018 in US. Residential sector produced more than 50%.

number of net metered PV installations on their systems between 2013 to 2016 [5]. Distributed generation from PV (which will be integrated at distribution level) is expected

to comprise 50%–60% of total U.S. PV capacity by 2020 [6]. Distributed PV systems connected to low/medium voltage distribution systems in the form of distributed generation (DG) have led to operational issues with increasing penetration levels [7]–[13].

Generating power locally using distributed energy resources (e.g. PV) causes power to flow in the reverse direction i.e. from house to the transformer. Reverse power flow brings several interconnection challenges, especially in the low voltage distribution grid. Voltage rise is one of the major challenges that limit the PV integration capacity in the feeder [14]. Fig. 1.2 shows the overvoltage scenario caused by the generation of power locally. The amount of voltage rise depends upon the net injected active and reactive power as well as on the distribution feeder parameters. The voltage rise can be approximated by (1.1) for a house connected to the substation by a feeder having resistance R and reactance X [14]. Here P, Q, and V are the net injected active power, net injected reactive power, and voltage at the substation respectively. Fig. 1.3 shows the

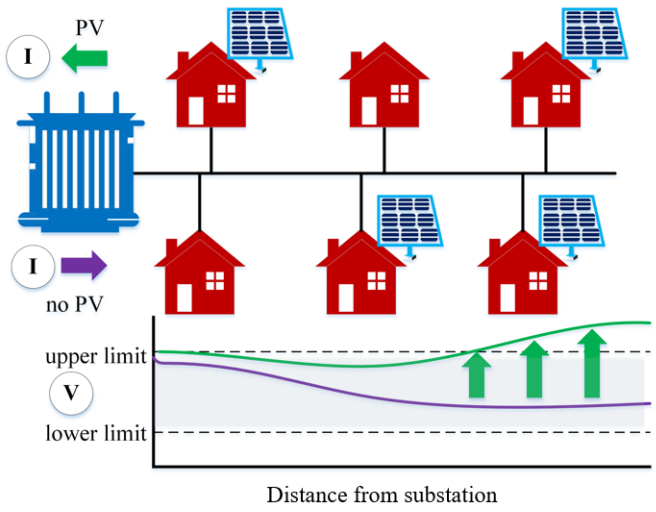

Figure 1.2. Schematic of distribution feeder supplied using off tap distribution transformer. Houses with PV panels can inject power during day time when generation is higher than load and may cause voltage rise. Note the drop in voltage magnitude down the feeder in the absence of PV.

interconnection of the residential house with a PV unit to the distribution grid. The solar energy from the sun is converted into electricity by a solar panel. The amount of power produced depends upon the amount of solar irradiance (measured in watt/m^2) hitting the solar panel normally, area of the solar panel and efficiency of the power conversion.

$$\Delta V = \frac{PR + QX}{V} \tag{1.1}$$

The PV inverter converts direct current (DC) electricity to alternating current (AC) electricity. The meter is connected just before the point of interconnection to the grid. The electricity can flow both in and out from residential home. For e.g. during an afternoon when power generation is high and consumption at a house is low, power flows from the house to the grid wheres during an evening in the absence of generation residential load receives power from the grid.

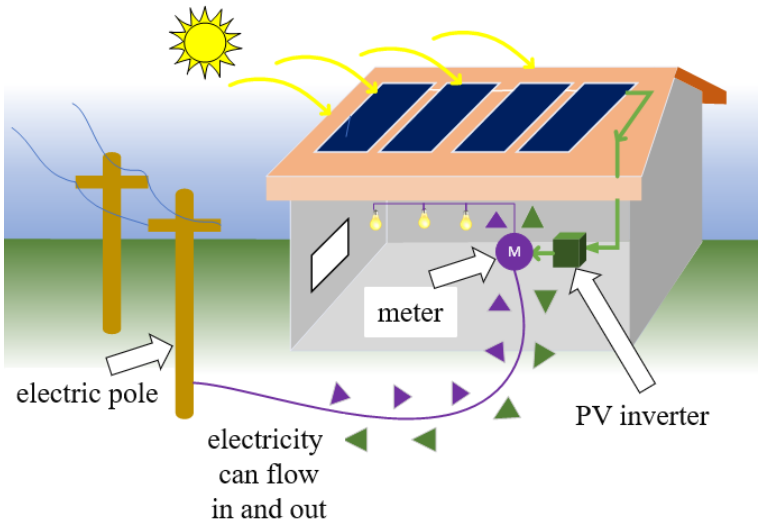

Figure 1.3. Schematic of residential house with rooftop PV and its grid interconnection. PV is connected to the electric grid via inverter and meter.

The rise of voltage caused by the local power generation has several negative

impacts on the operation of the power distribution system. Higher voltage increases feeder and transformer loss, increases the temperature deteriorating life and insulation of the electrical equipment and causes frequent tripping of the inverters. The traditional voltage regulating devices, such as line voltage regulators [15], switched capacitor banks [16], and on-load tap changing transformers cannot act in a sufficiently short time interval and result in poor regulation [17]. Even if these approaches could limit the voltage fluctuations, the high number of switching operations would shorten their operational life. As an alternative, utilities can increase the conductor size (decrease conductor resistance) of distribution lines to reduce voltage-rise, but upgrading the distribution system is not always economically viable [18].

New voltage control strategies need to be explored for better regulation. Fig. 1.4 gives a pictorial representation of ideal characteristics of voltage control strategy. The ideal voltage control strategy provides higher utilization of distribution system with minimal system impacts without conflicting pre-existing controllers with simple control scheme requiring minimal information and maximizes economic, environmental and societal benefits. Several studies have been done in the past decade to resolve integration challenges - particularly in the area of inverter control to prevent overvoltage. As modern inverters are smart enough to adjust their active and reactive power output and are already pre-installed during PV installation period, controlling inverter is the most straightforward solution to any integration challenge.

Popular approaches in network independent PV inverter overvoltage control are active power curtailment (APC) based on voltage deviations [14], [19], reactive power absorption based on linear Volt/Var droop [20], [21], and combined active-reactive power

Figure 1.4. Features of ideal voltage control strategy with increasing penetration of distributed generation.

management using limited communication [22]. However, long-term techno-economic and sustainability studies of such inverter controllers comparing different methods are still missing from the literature. One reason is the use of computationally burdensome electromagnetic transient (EMT) simulators to test the inverter controllers for preventing overvoltage, such as in [14], [19], [22], [23]. Long-term studies are important to make a better decision about the type of control strategy we want to adopt.

Different inverter control strategies to prevent overvoltage in PV rich distribution network are used to test proposed framework to assess their techno-economic and sustainability over the long run to help utility as well as consumers to decide which one is better for them. Voltage profile, transformer loading, energy generation, utility electricity sale and payback period have been analyzed using year-long simulation in minute

resolution to compare the techno-economic performance of five different PV inverter controllers. Three different sustainability metrics are proposed to assess their social, economic and environmental sustainability and multi-objective optimization is formulated to trade off between proposed sustainability metrics. Lastly, a concept of marginal cost is introduced to provide incentives for distribution ancillary services such as active power curtailment and reactive power absorption. In addition, a Monte-Carlo based PV hosting capacity analysis for a taxonomy feeder using High-Performance Computing is also included in the last Chapter to complete this thesis.

1.2 Related Work

The autonomous voltage control strategies are becoming popular to mitigate overvoltage caused by increasing PV installation in the distribution feeder. These control strategies have different impacts on the overall performance of the distribution system. The investment and operational costs for conventional grid extension measures with those resulting from the application of autonomous voltage control strategies over a period of 10 years, using real measured load and generation data have been analyzed to perform economic analysis in [24]. Results showed that implementing autonomous voltage control strategies can surely defer the grid investment cost. Similarly, implementation of autonomous voltage control strategies such as the droop based and ON/OFF PV inverter controllers cause unfair energy curtailment between PV units depending upon the location where PV is installed in the distribution feeder.

Unfairness in curtailed energy is measured by taking the standard deviation of normalized curtailed energy with respect to inverter ratings in and secondary voltage

control is proposed to mitigate such fairness in [25], however, the metric does not include local load which can have a huge impact on the unfairness. Active power management schedule based on self-consumption ratio – defined as the ratio of self-consumed energy to total energy produced, which treats each PV house in a fair way is proposed in [26]. Sensitivity information of the distribution network is exploited to provide fair energy curtailment in [27]. However combined study of unfairness, economic and environmental benefit of different autonomous inverter control strategies for voltage regulation is missing in the literature. We need active power curtailment and/or reactive power absorption to mitigate overvoltage caused by high PV penetration. These are sort of ancillary services that PV user can provide to maintain reliable distribution system operation. However, they cost money directly or indirectly. The concept of the locational marginal price for distribution grid (DLMP) is being studied in the literature [28]–[30]. However, studies of the locational marginal price for these ancillary grid services are missing. Locational marginal price can be used to provide incentives to anyone who is willing to providing these services.

1.3 Objective

The objective of the thesis was to develop a framework for assessing the techno-economic and sustainability aspect of the PV inverter control techniques which are meant to prevent overvoltage caused by reverse power flow from PV. A concept of locational marginal price for distribution grid ancillary services such as active power curtailment and reactive power absorption have also been studied in this research work. Additionally, a Monte Carlo based PV hosting capacity analysis was also performed in

taxonomy feeder using High-Performance Computing to show overvoltage effect at different PV penetration level. Following tasks are proposed to achieve the above objectives. The motivation for such a study is to help utility as well as PV users to decide upon suitable inverter control techniques.

(a) Performing tech-economic comparison between five different PV inverter controllers using proposed framework
(b) Designing metrics to help assess the sustainability of PV inverter control techniques
(c) Formulating multi-objective optimization to maximize both sustainability bounded by power system constraints and use it to find a correlation between them to decide upon the trade-off
(d) Analyze the locational marginal cost of distribution ancillary services such as active power curtailment and reactive power absorption.
(e) Monte Carlo based PV hosting capacity analysis using High-Performance Computing

1.4 Contributions

The main contributions of the thesis are stated below:

(a) Framework for evaluating techno-economic and sustainability study of PV inverter controllers for overvoltage mitigation
(b) Proposed social, economic and environmental sustainability metrics for PV inverter control techniques and application of it in five different local inverter control techniques

(c) Formulation of multi-objective optimization to maximize sustainability metrics to aid in decision making

(d) Distribution locational marginal pricing for active power curtailment and reactive power absorption to propose a market model for distribution ancillary services

(e) Use of High-Performance Computing for PV hosting capacity analysis

1.5 Thesis outline

The thesis is organized as follows: Chapter 2 describes five different local inverter control techniques and proposed framework which will be used later chapters to assess their sustainability. Chapter 3 discusses the techno-economic comparison of five different PV inverter controllers proposed in Chapter 2. Chapter 4 is where sustainability metrics are proposed, compared for five different PV inverter controllers and multi-objective optimization is formulated to trade off between proposed sustainability metrics. Chapter 5 discusses additional work about the concept of the marginal cost of ancillary services in the distribution system and Monte-Carlo based PV hosting capacity analysis in Taxonomy Feeder using High-Performance Computing.

CHAPTER 2 OVERVIEW OF PV INVERTER CONTROLLERS

2.1 Introduction

Increasing PV power injection in low voltage distribution systems may cause reverse power flow from end-users to the distribution substation which is the main reason for the occurrence of overvoltage in the distribution feeder. For a given distribution system, overvoltage caused by increasing the amount of installed DG (e.g. PV) can be prevented by curtailing active power and/or absorbing reactive power. The active and reactive power is controlled by the PV inverter, which is already required by the system to convert DC power from PV to AC power, resulting in a low-cost method for overvoltage prevention. Some of the PV inverter control methods which are used in later chapters for the purpose of comparing sustainability metrics are discussed below[1].

2.2 IEEE standard inverter overvoltage protection

The simplest approach to control overvoltage is to shut down the inverter when the local voltage exceeds the defined threshold value. In the IEEE 1547 standard [31], the threshold value is defined as 1.1 p.u., or alternatively, can be set to the upper limit of the extreme operating range defined by the ANSI C84.1-1989 standard [32] (which is 1.058 p.u.). In this approach, the PV inverter operates at maximum active power, p_{mppt}, at a unity power factor until the voltage at the point of connection reaches a maximum threshold voltage, v_{th}. If the local voltage rises above v_{th}, the inverter output is set to 0.

[1]The implementation of PV inverter controllers was a joint work with Rupak Mahat who was Master Student at South Dakota State University from 2016-2018. I worked with him in developing the sensitivity based algorithm for handling numerical oscillation caused by direct implementation of droop based inverter controllers in QSTS on his developed distribution model. I implemented the active reactive droop controller on top of his model and modified sensitivity algorithm for it. The techno-economic analysis after implementing the inverter controllers was done jointly by me and Rupak.

The re-connection time for inverters after shutdown is required to be a minimum of five minutes [31]. Acronym OVP will be used later to refer to IEEE standard inverter overvoltage protection method of PV inverter control. Although simple, the major disadvantage of this approach is the large increase in total energy curtailment, especially with a high-level of installed PV, leading to reduced financial benefits for the owner. A more effective approach is to partially curtail the active power from the PV inverter based on the local voltage measurement, as explained in the next section.

2.3 Droop based PV inverter control

2.3.1 Active Power Curtailment

PV inverters can locally mitigate overvoltage by curtailing active power and/or absorbing reactive power. In the APC approach, the PV inverter curtails its active power output as a function of local voltage deviation from a given critical voltage, v_{cri}. The most common method for implementing APC is using a linear gain proportional to the deviation of the voltage from v_{cri}. Let p_{mppt} be the maximum PV power for a given solar irradiance (kW), m_p be the linear droop coefficient (kW/V), and v be the local grid voltage at the PV inverter (V). In linear droop-based APC (LDAPC), the PV active power output, p_{inv}, is given by [14]:

$$p_{inv} = \begin{cases} p_{mppt} - m_p(v - v_{cri}), & \text{if } v \geq v_{cri} \\ p_{mppt}, & \text{if } v < v_{cri} \end{cases} \tag{2.1}$$

Another approach for APC, proposed in [19], uses a *quadratic* droop. In the quadratic droop-based APC (QDAPC), the amount of active power curtailed is

proportional to the *square* of the deviation of the voltage from v_{cri}. By using the quadratic droop, the amount of active power that is curtailed is lower for small voltage deviations, resulting in less energy curtailment over time. Let s be the quadratic droop coefficient (kW/V^2); for QDAPC, p_{inv} is given by:

$$p_{inv} = \begin{cases} p_{mppt} - s(v - v_{cri})^2, & \text{if } v \geq v_{cri} \\ p_{mppt}, & \text{if } v < v_{cri} \end{cases} \tag{2.2}$$

2.3.2 Active-Reactive Droop

In the active-reactive droop (ARD) method, reactive power absorption is used in coordination with APC to locally prevent overvoltage.

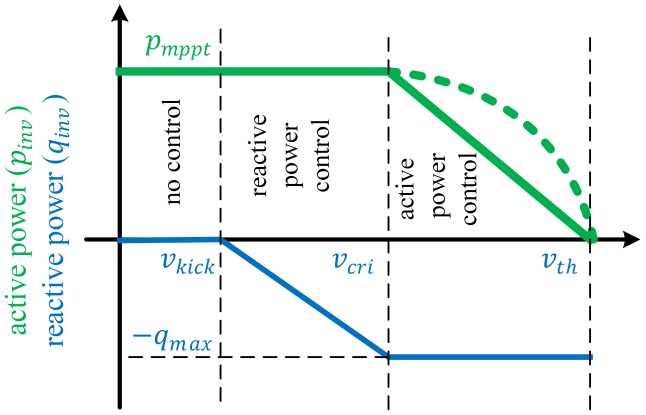

Figure 2.1. Variation of active and reactive power in droop-based PV inverter controllers. Solid green line for LDAPC, dotted green line for QDAPC and combination of solid green line blue solid line for ARD controllers.

Let v_{kick} be the voltage the inverter begins to absorb reactive power, m_q be the linear reactive droop (kVAR/V), and q_{max} be the maximum reactive power absorption (kVAR) — note that q_{max} depends on the inverter capacity and minimum allowable power factor (ϕ_{min}). The inverter reactive power, q_{inv}, is then given by (2.3), and p_{inv} follows (2.1). The

three droop-based PV inverter controllers are shown in Fig. 2.1, with LDAPC as the solid green line in the left figure, QDAPC in the dashed green line, and ARD in the right figure (where green shows APC and blue shows reactive power absorption).

$$q_{inv} = \begin{cases} 0 & v \le v_{kick} \\ m_q(v - v_{kick}) & v_{kick} < v < v_{cri} \\ -q_{max} & v \ge v_{cri} \end{cases} \tag{2.3}$$

2.4 Coordinated active reactive power management

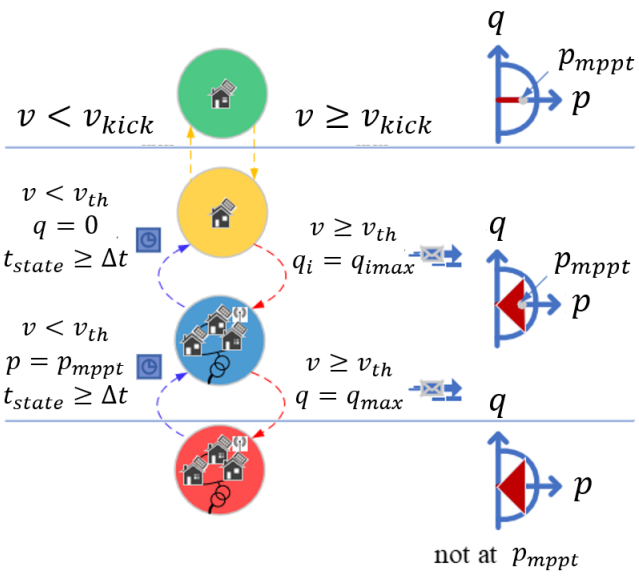

Figure 2.2. State transition diagram of the ARPM inverter controller.

The coordinated active and reactive power management (ARPM) controller uses the latent reactive power capacity of the inverters to attempt to correct overvoltage before starting to curtail active power [22]. A global communication signal (where APC and ARD methods are local) is used to coordinate distributed inverters to control active and

reactive power to prevent overvoltage. The ARPM state diagram is presented in Fig. 2.2. The green state represents normal operation ($v < v_{kick}$). If v goes above v_{kick}, the local inverter transitions to the yellow state to locally absorb reactive power. If the local reactive power support reaches its limit $q_i = q_{i,max}$ and local voltage is above v_{th}, a global communication signal is sent to all PV inverters to provide coordinated reactive power support (blue state). If the coordinated reactive power does not fix the overvoltage (i.e., $q = q_{max}$ for all inverters, $v \geq v_{th}$), all inverters begin curtailing active power (red state). Note that for transitioning from red to blue and from blue to yellow there is a time constant $t_{state} \geq \Delta t$ that suppresses fast transitions between states.

2.5 Numerical Oscillation of APC and ARD in QSTS

Implementing droop-based LDAPC, QDAPC, and ARD directly in QSTS results in numerical oscillation. Using such oscillatory voltage and power magnitudes to perform techno-economic and sustainability study leads to inaccurate results. In Section 2.5.1, benchmark system used and co-simulation framework for oscillation study is explained, and explanation to such oscillation is provided in Section 2.5.2.

2.5.1 Benchmark and Co-simulation Setup

For explanatory purposes, a radial feeder distribution system consisting of 12 house as shown in Fig. 2.3 is considered [14] and three droop based PV inverter controllers (LDAPC, QDAPC, and ARD) are implemented on top of it. The feeder is 120 m long, with two live wires twisted around a grounded neutral cable (NS 90 3/0 AWG). The service entrance consists of two wires supported by a steel grounded neutral cable (NS 90 1/0 AWG). Each house in the distribution feeder is 20 m from the main distribution line.

The line parameters of the benchmark feeder are provided in [14]. The feeder and transformer parameters are presented in Table 2.1.

Table 2.1. Feeder and transformer parameters

	resistance	reactance
feeder backbone	1.114 Ω/mile	0.291 Ω/mile
feeder lateral	1.767 Ω/mile	0.279 Ω/mile
transformer (referred to secondary)	0.018 Ω	0.045 Ω

A QSTS, GridLAB-D [33], was used to develop a distribution system model for this convergence study. An external controller written in Python was used to exchange data with GridLAB-D through Bus.py [34] during runtime to enable implementation of the PV inverter controllers in GridLAB-D. Other simulation parameters are listed in Table 2.2.

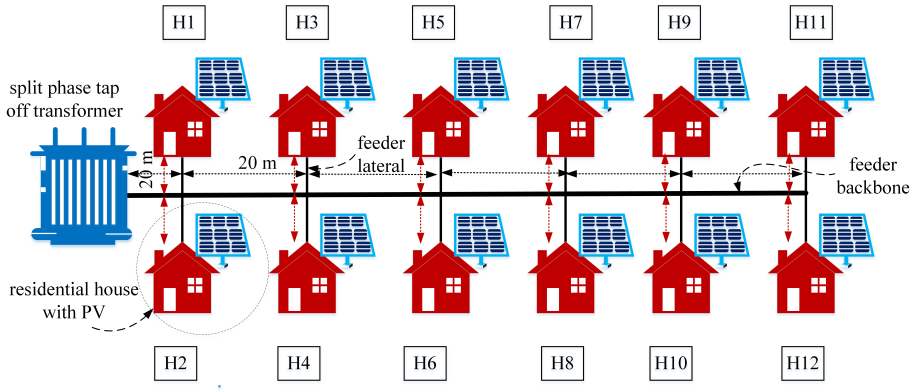

Figure 2.3. Single line diagram of 12 house radial feeder with grid-connected PV installed at each house supplied using split phase off tap distribution transformer.

Table 2.2. Simulation Parameters

Parameter	Value
$v_{th}, v_{cri}, v_{kick}$	1.058, 1.042, 1.02 p.u.
m_p, s, m_q	2.1 kW/V, 0.57 kW/V^2, 0.523 kvar/V
q_{max}, ϕ_{min}	2.761 kvar, 0.95

2.5.2 Explanation to Oscillation

The PV power of each house in the 12 house benchmark is changed from 0 kW to 6.25 kW with all three controllers The resulting numerical oscillations caused by the controller response at farthest houses (H11/12) are shown in Fig. 2.4. For other houses, the oscillation will be smaller but follows the same pattern. When implementing the droop-based controllers in QSTS, system dynamics are neglected during the discrete time-steps. The implemented droop controllers thus generate control actions from steady-state RMS values at every iteration, causing numerical oscillation from large changes in V in one time-step, Δt.

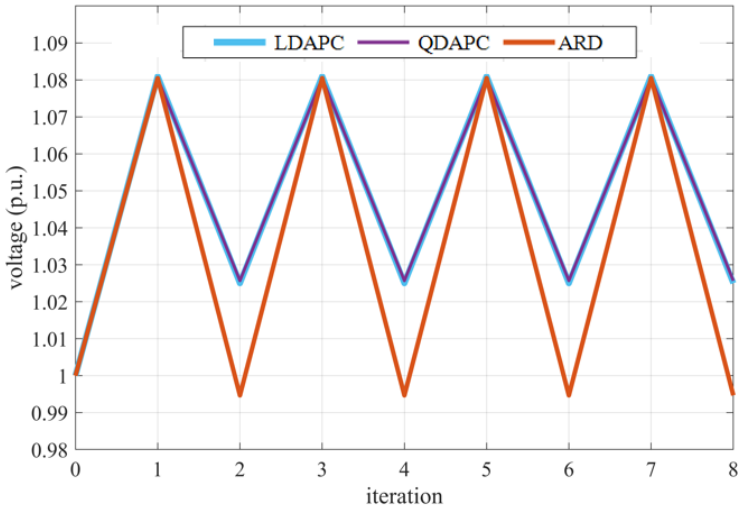

Figure 2.4. Voltage numerical oscillation in droop based PV inverter controllers (LDAPC, QDAPC and ARD) when maximum available power (p_{mppt}) is changed from 0 kW to 6.25 kW for farthest houses (H11/12).

When the local voltage v is high for time-step t, the PV APC is high in time-step $t+1$ in the QSTS based on (2.1) for LDAPC — similarly for QDAPC from (2.2) and reactive power absorption in ARD from (2.3). The high PV APC, in turn, leads to a significant drop in voltage, which causes the controller to again inject p_{mppt}. The

oscillation continues indefinitely as shown in Fig. 2.4, with higher oscillations for houses located further from the substation.

2.6 Proposed Sensitivity-based Algorithm

2.6.1 Algorithm for APC Controller

For solving the numerical oscillation problem, a sensitivity-based technique is proposed to iteratively determine p_{inv} and q_{inv} for each PV inverter at each discrete time-step in the QSTS. The proposed technique is described in Algorithm 1 for the LDAPC controller. At the beginning of a simulation, the parameters (initial voltage, critical voltage, initial APC, and droop coefficient of each inverter) are initialized as shown in the initialization block. After initialization, for each time-step of the QSTS simulator, the active power output of each PV inverter is iteratively determined using a sensitivity matrix derived from the distribution network parameters and the distribution system state.

Let v and δ be the voltage magnitude and angle at a distribution bus, respectively, and p and q be the net injected active and reactive power, respectively. The oscillation issue can be addressed by determining APC using a voltage sensitivity index ($\Delta v/\Delta p$), which estimates the change in voltage due to a corresponding change in active power injection. The amount of curtailment is iteratively calculated during subsequent time-steps until the voltage converges to a steady-state value. A sensitivity matrix for a power system network ($\mathbf{S_V}$) consists of partial derivatives that represent the change in voltage magnitude and angle ($\Delta v, \Delta\delta$) of each bus due to the changes in active and reactive power ($\Delta p, \Delta q$) at each bus.

For an n-bus power system network, the voltage sensitivity matrix in compact

notation can be written as in (2.4).

$$\mathbf{S_V} = \begin{bmatrix} (\frac{\Delta\delta}{\Delta p}) & (\frac{\Delta\delta}{\Delta q}) \\ (\frac{\Delta v}{\Delta p}) & (\frac{\Delta v}{\Delta q}) \end{bmatrix}_{2n\times 2n} \tag{2.4}$$

A sensitivity matrix, **A**, of the change in voltage magnitude with respect to the active power can be defined as a submatrix of the voltage sensitivity matrix.

$$\mathbf{A} = \left[\frac{\Delta v}{\Delta p}\right]_{n\times n} \tag{2.5}$$

Let $\mathscr{N} := \{2,3,....n\}$ be the set of distribution system buses, not including the slack bus. We define $\mathscr{N}_g \subseteq \mathscr{N}$ as a collection of buses where DG (PV in this case) is connected, and $H = |\mathscr{N}_g|$. Let $\mathbf{S_p}$ be an $h \times h$ sensitivity matrix with element $\mathbf{S_p}(\mathbf{i},\mathbf{j}) \in \mathbf{A}$ corresponding to the sensitivity of DG bus i with respect to DG bus j, $\forall\, i,j \in \mathscr{N}_g$.

At iteration k, let $\mathbf{v}^{(k)}$ and $\mathbf{v_{cri}}$ be vectors of size h containing the measured voltage magnitude at each PV inverter and the critical voltage, respectively, and $\mathbf{p_c}^{(k)}$ be a vector of size H of the active power curtailed at each PV inverter. To calculate the curtailed active power at iteration k, we set

$$\mathbf{p_c}^{(k)} = \mathbf{p_c}^{(k-1)} + \Delta\mathbf{p_c}^{(k)}, \tag{2.6}$$

where $\Delta\mathbf{p_c}^{(k)}$ is the change in active power curtailed from iteration $k-1$ to k calculated as:

$$\Delta\mathbf{p_c}^{(k)} = \mathbf{B_p}^{-1}\mathbf{a_p} \tag{2.7}$$

where $\mathbf{a_p} = m_p(\mathbf{v}^{(n)} - \mathbf{v_{cri}}) - \mathbf{p_c}^{(k-1)}$, $\mathbf{B_p} = m_p\mathbf{S_p} + \mathbf{I}$, and $\mathbf{I}$ is the identity matrix. The derivation of $\Delta\mathbf{p_c}^{(k)}$ is shown in Appendix A.

After calculating $\Delta\mathbf{p_c}^{(k)}$, APC is obtained using (2.6). Let $\mathbf{p_{mppt}}$ be a vector of size h denoting the maximum active power available at each PV inverter, $\mathbf{p_{inv}}$ be a vector of size h denoting the active power output of each PV inverter, and $\mathbf{c}$ be a binary vector of size h where each element is $\in \{0,1\}$ based on $\mathbf{v}^{(n)} \geq \mathbf{v_{cri}}$.

Algorithm 1: Implementing the LDAPC Controller

Input:

- Critical Voltage: $\mathbf{v_{cri}}$
- Active droop coefficient: m_p
- Initial Inverter voltage: $\mathbf{v}^{(k)}$
- Initial Curtail power: $\mathbf{p_c}^{(k)}$

Data:

- Read PV power $\mathbf{p_{mppt}}$
- Read house load power

while $||\mathbf{v}^{(k)} - \mathbf{v}^{(k-1)}||_\infty > \varepsilon$ **do**
  $\Delta\mathbf{p_c}^{(k)} = \mathbf{B_p}^{-1}\mathbf{a_p}$
  $\mathbf{p_c}^{(k)} \leftarrow \mathbf{p_c}^{(k-1)} + \Delta\mathbf{p_c}^{(k)}$
  $\mathbf{p_{inv}^{(k)}} \leftarrow \mathbf{p_{mppt}} - \mathbf{c} \odot \mathbf{p_c^{(k)}}$
  solve load flow with $\mathbf{p_{inv}}^{(k)}$
  $k \leftarrow k+1$
end
return $\mathbf{p_{inv}}$

At each iteration n, the PV inverter power is set to $\mathbf{p_{inv}^{(k)}} = \mathbf{p_{mppt}} - \mathbf{c} \odot \mathbf{p_c^{(k)}}$ (i.e., $\mathbf{p_{mppt}}$ if $v < v_{cri}$, otherwise curtailed according to $\mathbf{p_c}^{(k)}$). The algorithm continues until $||\mathbf{v}^{(k)} - \mathbf{v}^{k-1)}||_\infty \leq \varepsilon$, where $\varepsilon > 0$ is a stopping tolerance. After convergence, p_{inv} is set for each PV inverter in the QSTS. The algorithm is similar for QDAPC, with slight

modifications given in Appendix B.

2.6.2 Algorithm for ARD Controller

The sensitivity-based algorithm for the ARD controller is presented in Algorithm 2. Because ARD absorbs reactive power in addition to curtailing active power, the voltage magnitude sensitivity with respect to reactive power must also be included. Let $\mathbf{B}$ be the submatrix that indicates nodal sensitivity of voltage magnitude with respect to reactive power.

$$\mathbf{B} = \left[\frac{\Delta v}{\Delta q}\right]_{n\times n} \tag{2.8}$$

Let $\mathbf{S_q}$ be an $h \times h$ sensitivity matrix with element $\mathbf{S_q}(\mathbf{i},\mathbf{j}) \in \mathbf{B}$ corresponding to the sensitivity of DG bus i with respect to DG bus j, $\forall\, i, j \in \mathcal{N}_g$; $\mathbf{v_{kick}}$ be a vector of size h of kickoff voltages; and $\mathbf{q_a}^{(k)}$ be a vector of size h of the reactive power absorbed at each PV inverter. To calculate the reactive power absorption at iteration k, we set

$$\mathbf{q_a}^{(k)} = \mathbf{q_a}^{(k-1)} + \Delta\mathbf{q_a}^{(k)}, \tag{2.9}$$

where $\Delta\mathbf{q_a}^{(k)}$ is the change in reactive power absorbed from iteration $k-1$ to k calculated as:

$$\Delta\mathbf{q_a}^{(k)} = \mathbf{B_q}^{-1}\mathbf{a_q} \tag{2.10}$$

where $\mathbf{a_q} = m_q(\mathbf{v}^{(k)} - \mathbf{v_{kick}}) - \mathbf{q_a}^{(k-1)}$, and $\mathbf{B_q} = m_q\mathbf{S_q} + \mathbf{I}$. To compute APC, a slight modification is necessary (as the PV inverter is set to q_{max}), where $\Delta\mathbf{p_c}^{(k)}$ will be calculated using (2.11).

$$\Delta \mathbf{p_c}^{(k)} = \mathbf{B_p}^{-1} \mathbf{a_p^*} \tag{2.11}$$

where $\mathbf{a_p^*} = m_p(\mathbf{v}^{(k)} - \mathbf{v_{cri}} - \mathbf{S_q q_{max}}) - \mathbf{p_c}^{(k-1)}$, and $\mathbf{q_{max}}$ is the vector of size h containing the maximum reactive power each inverter can absorb. The derivation of $\Delta \mathbf{q_a}^{(k)}$ and $\mathbf{a_p^*}$ are shown in Appendix B. Like $\mathbf{c}$, $\mathbf{c_q}$ is a binary vector of size h where each element is $\in \{0, 1\}$ based on $\mathbf{v}^{(k)} \geq \mathbf{v_{kick}}$. The remainder of Algorithm 2 works as explained in Section 2.6.1.

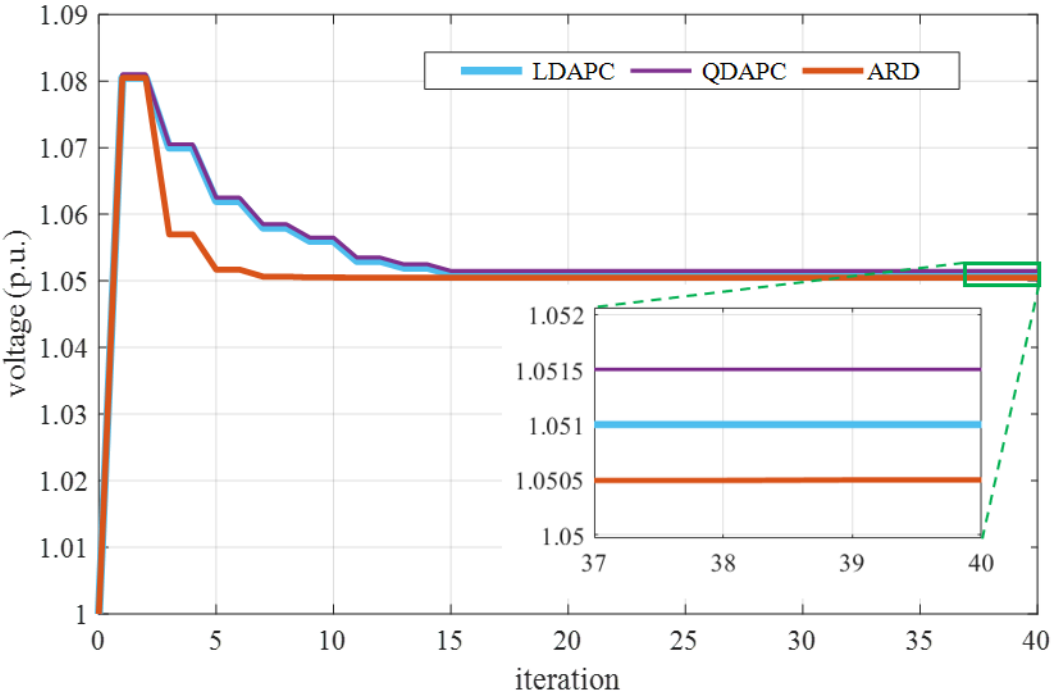

Figure 2.5. Convergence of voltage magnitude in three droop based PV inverter controllers LDAPC, QDAPC and ARD when maximum available PV power (p_{mppt}) changes from 0 kW to 6.25 kW for farthest houses (H11/12).

2.6.3 Algorithm Convergence

Fig. 2.5 shows the convergence of the sensitivity-based algorithms for the farthest houses in the benchmark (H11/12) for LDAPC, QDAPC, and ARD, given in cyan, magenta, and orange, respectively.

Algorithm 2: Implementing the ARD controller

Input:

- $\mathbf{v_{cri}}$, m_p,$\mathbf{v}^{(k)}$, $\mathbf{p_c}^{(k)}$
- Kickoff voltage $\mathbf{v_{kick}}$
- Initial reactive power absorption: $\mathbf{q_a}$
- Reactive droop coefficient: m_q

Data:

- Read $\mathbf{p_{mppt}}$, house load power

while $||\mathbf{v}^{(k)} - \mathbf{v}^{(k-1)}||_\infty > \varepsilon$ **do**
  $\Delta\mathbf{p_c}^{(k)} = \mathbf{B_p}^{-1}\mathbf{a_p^*}$
  $\mathbf{p_c}^{(k)} \leftarrow \mathbf{p_c}^{(k-1)} + \Delta\mathbf{p_c}^{(k)}$
  $\mathbf{p_{inv}^{(k)}} \leftarrow \mathbf{p_{mppt}} - \mathbf{c} \odot \mathbf{p_c^{(k)}}$
  $\Delta\mathbf{q_a}^{(k)} = \mathbf{B_q}^{-1}\mathbf{a_q}$
  $\mathbf{q_a}^{(k)} \leftarrow \mathbf{q_a}^{(k-1)} + \Delta\mathbf{q_a}^{(k)}$
  $\mathbf{q_{inv}^{(k)}} \leftarrow -\mathbf{c_q} \odot \mathbf{q_a^{(k)}}$
  if $\mathbf{q_{inv}^{(k)}} \geq \mathbf{q_{max}}, \mathbf{q_{inv}^{(k)}} \leftarrow -\mathbf{q_{max}}$
  solve load flow with $\mathbf{p_{inv}}^{(k)}$ and $\mathbf{q_{inv}}^{(k)}$
  $k \leftarrow k+1$
end
return $\mathbf{p_{inv}}$ and $\mathbf{q_{inv}}$

Note in each iteration, the voltage change is greater for ARD than LDAPC and QDAPC, because ARD uses both reactive power absorption and active power curtailment for voltage control. All controllers converged in less than 15 iterations. Compared to Fig. 2.4, the numerical oscillations are eliminated using the iterative sensitivity-based

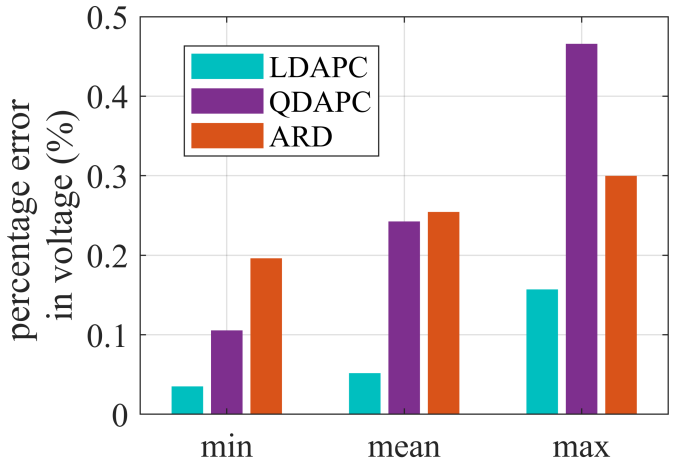

Figure 2.6. Absolute percent error in voltage magnitudes for farthest houses (H11/12) between GridLAB-D and PSCAD when implementing droop based inverter controllers (LDAPC, QDAPC, and ARD) with the proposed sensitivity-based algorithm.

approach. The results are similar to the other houses. To check the solution of the accuracy of the converged voltage magnitude using the sensitivity-based algorithm, dynamic simulations of these controllers in the same benchmark were conducted in PSCAD. The dynamic model of the benchmark in PSCAD was first validated against the GridLAB-D model without PV controllers by matching nodal voltage magnitudes with different active power injection levels. The PV controller outputs were then tested using ten different active power injection levels — varying from 20 kW to 75 kW in a step of 5kW. These values were chosen because net generation below 20kW did not cause curtailment, above 75 kW is limited by transformer capacity. All cases were run separately in GridLAB-D and PSCAD, and the min, mean, and max percent error in voltage magnitude were compared for the farthest houses (H11/12).

The errors for each of the three PV inverter controllers are shown in Fig. 2.6, with the maximum absolute error in voltage limited to below 0.5% in all controllers. The minor difference in PV controller converged values may be due to the different network

equations solved by the QSTS (steady-state RMS values) versus dynamic (measured RMS values). The minor differences are acceptable for the domains that are studied using QSTS (e.g., energy costs, steady-state voltage).

2.7 Framework for Techno-Economic and Sustainability Study

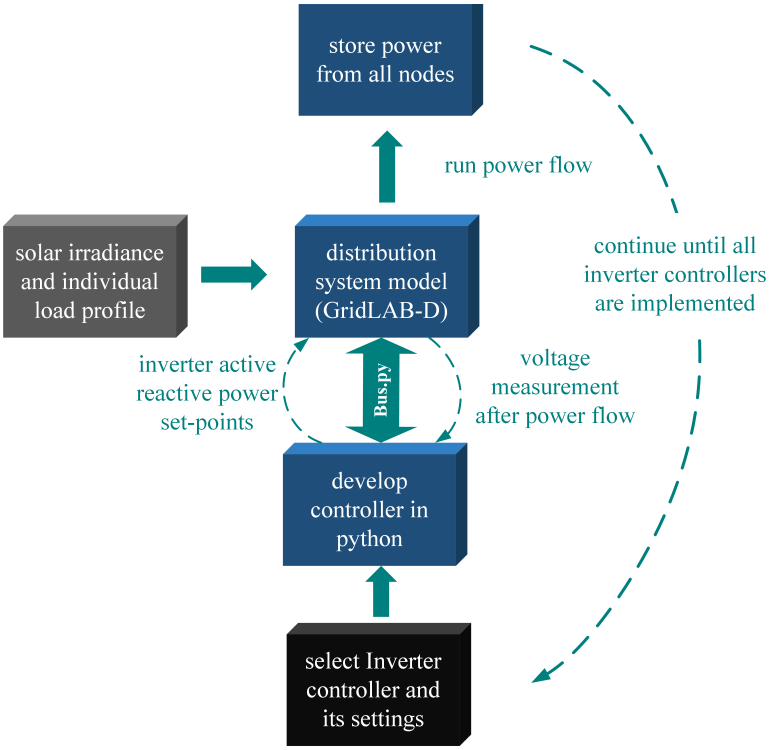

Figure 2.7. Framework for evaluating PV inverter controllers for voltage regulation. All controllers are implemented in python which will interact with GridLAB-D in run-time to change inverter set-points based on voltage measurements obtained after power flow. The voltage magnitudes and power measurements from all nodes after final power flow will be stored for post-processing helping to do techno-economic and sustainability assessment.

The general framework for techno-economic and sustainability study of PV inverter controllers for voltage regulation is shown in Fig. 2.7. The inverter controller under investigation is implemented in *python* (an open source programming language useful for computation, data visualization and many more) which will control the PV inverters modeled in GridLABD along with distribution feeders. GridLAB-D is a power system

modeling and simulation environment developed by the U.S. Department of energy [33]. GridLAB-D runs power flow by taking load data input for each load node in the feeder (note a solar inverter is modeled as a negative load). The inverter could not be implemented in GridLAB-D instead, python is used as a programming platform to implement PV inverter controllers. Co-simulation between python and GridLABD is performed using *Bus.py* [34], a python module, to exchange information between them. Voltage measurements from GridLAB-D are used by the controller to compute inverter active and reactive power set-points. These new inverter set-points will be used by GridLAB-D again to conduct power flow. Finally, power measurements from all nodes at all times will be collected. The process is continued for all PV inverter control schemes.

CHAPTER 3 TECHNO-ECONOMIC STUDY

The framework proposed in Chapter 2 is used to perform techno-economic and sustainability study in five different inverter control schemes explained in the same chapter. The chapter first describes the simulation methodology and then analyzes the results of techno-economic performance comparison[2].

3.1 Simulation Methodology

The five different PV inverter controllers described in Chapter 2 (OVP, LDAPC, QDAPC, ARD, and ARPM) are compared based on their long-term technical and economic impact in LV distribution systems. An annual simulation is performed using input data for the year 2014. The section describes the benchmark, input data for load, irradiance, and electricity pricing, and provides the PV controller parameters used in the simulation study. The values are chosen for this comparative techno-economic study, but the methods are general enough to be used for any combination of input parameters, distribution network, and PV inverter controller. The co-simulation and benchmark for implementing PV inverter controllers are already explained in Chapter 2.

3.1.1 Load Data

Unique load data was created for each house using the $M_t/G/\infty$ queue model from [35]. The model makes use of the openly available hourly load data from distribution companies to create unique random loads for each house that statistically aggregate to the known distribution system load profile. For the simulation, the 2014 annual load from

[2]The implementation of PV inverter controllers (OVP, LDPAC, QDAPC, and ARPM) along with distribution system modeling in GridLAB-D for techno-economic study is a joint work between Rupak Mahat – a former SDSU graduate, and Kapil Duwadi in year 2017-2018.

ComEd (Chicago, IL) was scaled down to a 100 W and 5000 W upper and lower bound, respectively, for the queue model. The year-long load profile for H12 is shown in Fig. 3.1, along with a zoomed in version for one day. For other houses load profiles will follow a similar pattern.

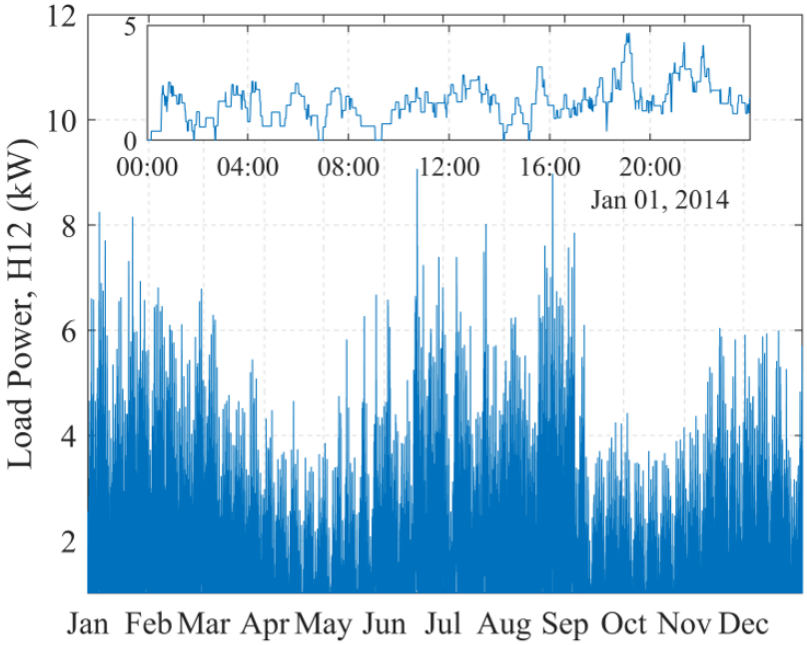

Figure 3.1. Year long load profile for farthest house (H12) in minute resolution with zoomed in view shown for one day to illustrate random load changes generated using queuing load modelling technique for 2014.

3.1.2 PV Data

Global horizontal irradiance data obtained from SolarAnywhere [36] is used to calculate hourly available PV power. The study considers Chicago, IL, at latitude 41.88° N and longitude 87.66° W for 2014 to match the synthetic load data and pricing information. Solar data required for the one-minute simulation timestep is calculated from the hourly data using linear interpolation. Let η be the efficiency of the PV panel, I be the solar irradiance $(\mathrm{W/m^2})$, and A be the area of the PV panel $(\mathrm{m^2})$. Irradiance data is then used to

calculate the maximum power available in the PV array as $P_{MPPT} = \eta \times I \times A$. For an 8.4 kW capacity PV system, the efficiency is taken as η =16.7% and A =50.2605 m^2 [37].

3.1.3 Utility Tariff Structures

Two tariff schemes, RTP and flat rate, are used to investigate economic impacts of the PV systems with different inverter controllers. Pricing information is obtained from ComEd for both tariff schemes to match the irradiance and load data for Chicago, IL. The end-users are assumed to be in a net metering program, where excess PV energy is sold back to the utility at the same rate paid for consumption. In both tariff schemes, the total charge paid by the end-user is divided into three categories: supply charge, delivery charge, taxes, and fees. The main difference between the two tariffs is in the supply charge; the energy charge for RTP is calculated based on the hourly RTP, averaged from 5-minute RTP blocks provided by ComEd [38], while the price is constant in the flat rate tariff. Additionally, the capacity charge included in the RTP scheme as part of the supply charge, which is computed based on the end user's contribution to the system peak load. The delivery charges, taxes, and fees are similar for both tariff schemes, but the flat rate tariff has an additional energy efficiency program charge.

3.1.4 Controller Parameters

The controller parameters for droop based PV inverter control schemes (LDAPC, QDAPC, and ARD) are the same as used in Chapter 2. For implementing the ARPM controller t_D and Δt are taken as 20 min. and 1 min. intervals respectively[22].

3.2 Results and Analysis

Results after technical and economic performance comparison are analyzed by looking at various performance indexes as explained below in detail.

3.2.1 Voltage Profile

The performance of the different inverter controllers for overvoltage prevention in LV distribution systems caused by increased PV installation is analyzed in this section using the parameters outlined above. A violin plot showing the annual distribution of voltage magnitudes for each controller, compared to the baseline case without overvoltage protection control (i.e., $p_{inv} = p_{mppt}$, regardless of voltage issues), is presented in Fig. 3.2 (6,307,200 voltage magnitude samples from all 12 houses using one-minute time resolution over one year). Violin plot is similar to a box plot but with the (rotated) kernel density plot on each side. The thickness (or density) represents how often each voltage magnitude occurred. The shape of the distribution of voltage magnitudes within the operating zone (for OVP, LDAPC, and QDAPC between 1.042 and 1.058 p.u., and for ARD and ARPM between 1.02 to 1.058 p.u.) reflects the controller response to overvoltage. If no overvoltage protection is implemented, the system will reach a peak voltage of 1.09 p.u. The minimum voltage in the system is 0.95 p.u. and remains unaffected by the implementation of the inverter controllers (note, preventing undervoltage is not within the scope of this paper).

The voltage magnitudes are clustered closer to the upper limit (1.058 p.u.) for QDAPC, whereas they are clustered near the lower limit (1.042 p.u.) in LDAPC. The ability of QDAPC to maintain the voltages near the maximum limit more often than

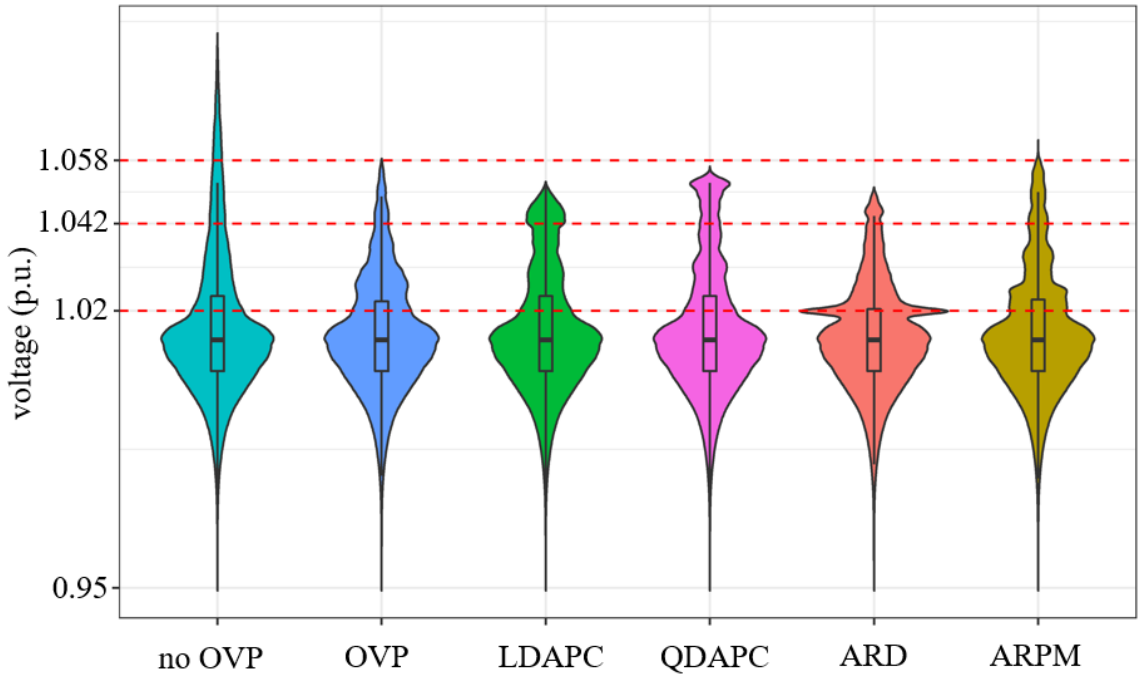

Figure 3.2. Distribution of voltage magnitudes in the form of violin plot for different five different PV inverter controllers compared to no overvoltage protection case for the year 2014. The controllers objective is to keep the voltage below 1.058 p.u.

LDAPC is because QDAPC curtails less active power for voltages near the lower limit (quadratic behavior). Thus, QDAPC greatly reduces total energy curtailment compared to the LDAPC while still maintaining the voltage within the limits. In the OVP inverter controller, because the inverter shuts down (full curtailment) and remains off for five minutes after the occurrence of overvoltage, the voltage immediately drops once overvoltage occurs.

The lower density of voltage magnitudes in the range between 1.042 p.u. and 1.058 p.u. in the ARD and ARPM controllers compared to LDAPC and QDAPC is because, in the region of interest, the controller is absorbing reactive power to avoid overvoltage while injecting maximum available power from the PV. The ARD controller is able to maintain the voltage below v_{th} compared to other controllers because the PV

inverter absorbs maximum reactive power after v_{cri}, whereas in ARPM this occurs after v_{th}. The high density centered at 1.02 p.u. in ARD controller is the cumulative effect of collecting voltage magnitude samples from each of the 12 houses. Note the definition of maximum reactive power is different in ARD and ARPM. In ARD, maximum reactive power is fixed and determined by inverter capacity, whereas in ARPM it is time-varying and dependent on p_{mppt} (ARD will always be greater than or equal to ARPM, allowing ARD to absorb more reactive power and thus lowering voltage).

All controllers are able to maintain the voltage below 1.058 p.u. except for the ARPM controller. The inability to maintain voltage magnitudes above 1.058 p.u. all time in ARPM controller is because of the inherent characteristics of the algorithm, in which the communication signal is issued only *after* the local voltage of a house reaches 1.058 p.u., and controller takes time for the other houses to ramp their reactive power absorption to the maximum limit and curtail active power when needed. In this simulation study, the local voltage at houses closer to the distribution transformer never exceeds the critical voltage (specifically H1–H4 for OVP, LDAPC, and QDAPC, and H1–H6 for ARD), indicating that local inverter controllers do not curtail active power. In the ARPM controller, these houses curtail to prevent overvoltage as ARPM takes a coordinated approach.

3.2.2 Energy Generation and Consumption

In Fig. 3.3, five different colored dots for each house illustrate the annual energy being generated by a house with the five different inverter control methods for 2014. The bar graph overlaid in the lower left represents the annual aggregated energy being

generated by the 12 houses. The total generated energy is greatest with the ARD and ARPM controllers because they both absorb reactive power as the first strategy to mitigate overvoltage; active power is curtailed only if the reactive power capabilities are not sufficient to prevent the overvoltage. The lower total energy generation in ARD compared to ARPM is because the former uses the same droop coefficients for each house based on local voltage, whereas the latter uses a communication signal to coordinate reactive power support from all PV inverters. Tuning the ARD coefficients might increase the total generated energy and could be further evaluated using the proposed framework.

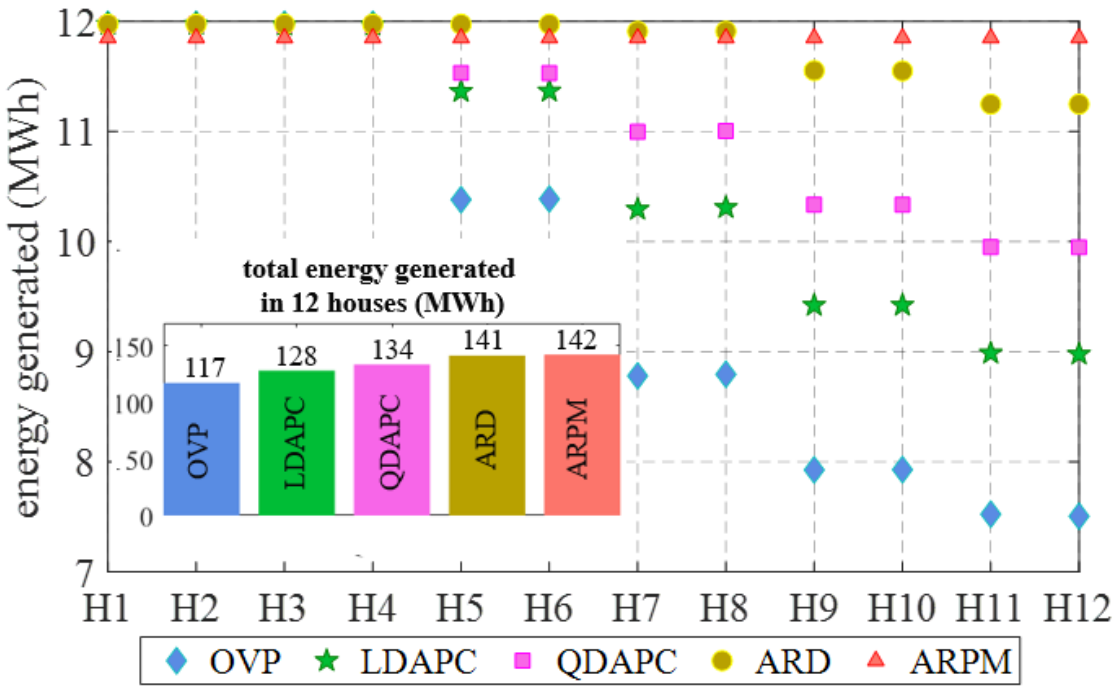

Figure 3.3. House-wise energy generation from PV for the year 2014 for five different PV inverter controllers. Overlay bar graph shows controller-wise aggregated annual energy generation for the same year. The variation in energy generation is higher in OVP and least in ARPM between houses with a total generation being highest.

Among the droop-based APC controllers, QDAPC produced the highest energy compared to LDAPC. By curtailing the active power proportional to the square of voltage

deviation in QDAPC, less active power is curtailed when the voltage is near v_{cri}, allowing QDAPC to curtail less energy than LDAPC. OVP controller has the least amount of energy generation because the inverter shuts down to prevent overvoltage, causing full curtailment of the available PV power. Additionally, the inverter remains off for five minutes after the overvoltage has occurred.

Fairness is observed — all houses curtail the same amount of active power — in energy generation for each of the 12 houses if using the ARPM controller because of the coordinated reactive power absorption and active power curtailment strategy. Fairness is important from the user point of view, as energy generated is independent of the location of the house on the power network and can be used to quantify a social aspect of the controllers discussed in detail in Chapter 4. Energy generated is not fair among houses for the other controllers as they make local decisions, which are greatly influenced by location on the network. However, the controller might not lead to minimum curtailment at the system level, which needs to be further investigated. Except for ARPM, generation significantly reduces with the distance from the transformer in other controllers. On the other hand, total energy generated by houses close to the substation transformer is the same, with a slight reduction in energy generation with ARPM controllers (caused by coordinated active power curtailment, where houses may curtail before they have a local voltage issue).

The local generation of energy using PV helps in reducing electric energy consumption (demand). In Fig. 3.4, each dot represents the net annual energy consumed by the house, with different colors representing the different inverter controllers (except for cyan colored dots, which represent energy consumption without PV). The bar graph

overlaid in the left represents the aggregated annual energy consumption of all 12 houses for different controllers. The energy consumed significantly decreased with the

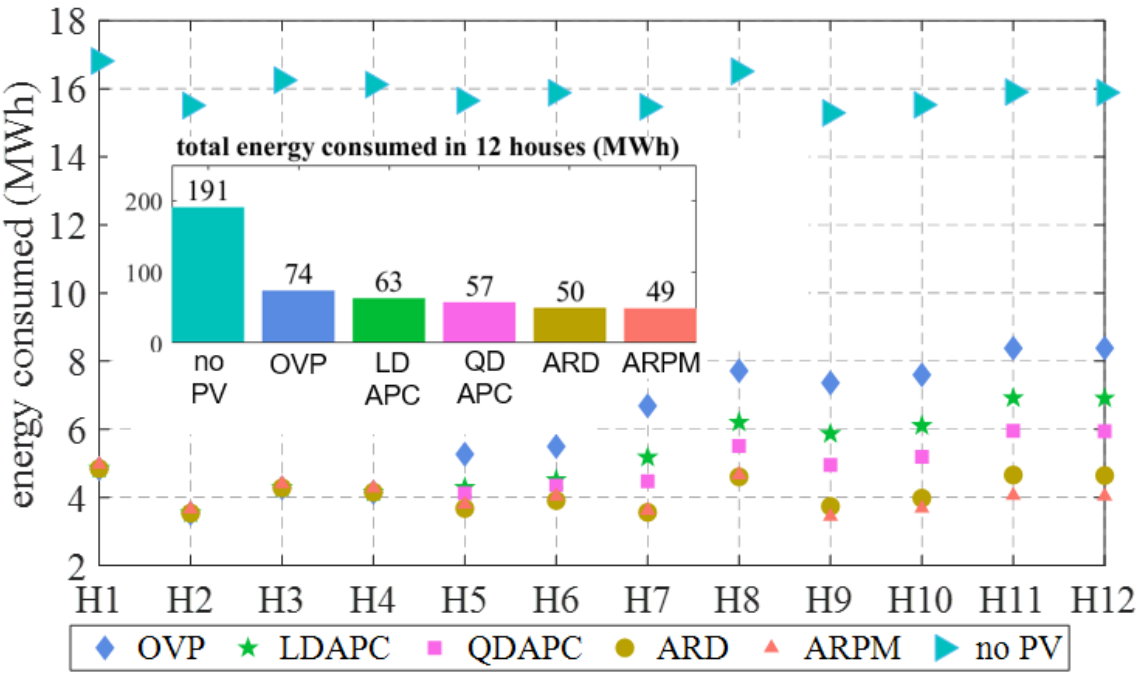

Figure 3.4. House-wise net annual energy consumption in five different PV inverter controllers for the year 2014 compared to no PV case. Overlaid bar graph shows controller-wise aggregated annual energy consumption for the same year. Net energy consumption reduced greatly with PV and highest reduction achieved in ARPM controller.

installation of a PV system in all houses, directly leading to economic benefits for the owner. ARD and ARPM had similar results from the point of view of total energy consumed. If reactive power could not be used, LDAPC or QDAPC would lead to approximately 15-30% increase in energy consumption. Considering OVP, the disconnection time after overvoltages led to higher household energy provided from the utility — close to a 50% increase compared to ARD and ARPM, as shown in Fig. 3.3. The variation in different household energy consumption in the no PV and ARPM cases are from the randomness of the load generation from the queue model.

3.2.3 Energy Losses

Energy loss is another pertinent technical consideration to assess the performance of inverter overvoltage prevention controllers. The distribution system energy losses are divided into transformer losses and distribution line losses. The transformer losses only include the loss in equivalent series impedance. Actual transformer losses will be slightly higher as shunt parameters are neglected. However, neglecting shunt parameter will not affect the comparison study, because the change in no-load loss due to the controllers is insignificant compared to the change in series losses. In this study, the distribution and transmission systems losses before the LV transformer are not considered.

In Fig. 3.5, the annual distribution system losses for different controllers are shown, compared to the same system without installed PV. The higher distribution energy losses from ARPM and ARD is due to higher active power injection and reactive power absorption. The slightly higher feeder and transformer losses in ARD compared to ARPM is because the PV inverter absorbs greater than or equal reactive power than ARPM at a given voltage due to the tuning of the droop coefficients. Transformer losses contributed to almost 40% of the total distribution loss in the system. The higher energy loss in droop-based APC controllers (both LDAPC and QDAPC) than OVP is because of the higher energy being injected from PV by these controllers.

In the no PV case, the total distribution energy loss is lower for all controllers, except loss is slightly higher than OVP. The higher losses in the distribution system as compared to the no PV case can be attributed to the fact that load and PV generation do not often correlate leading to more periods of high current flowing in the feeder, which in

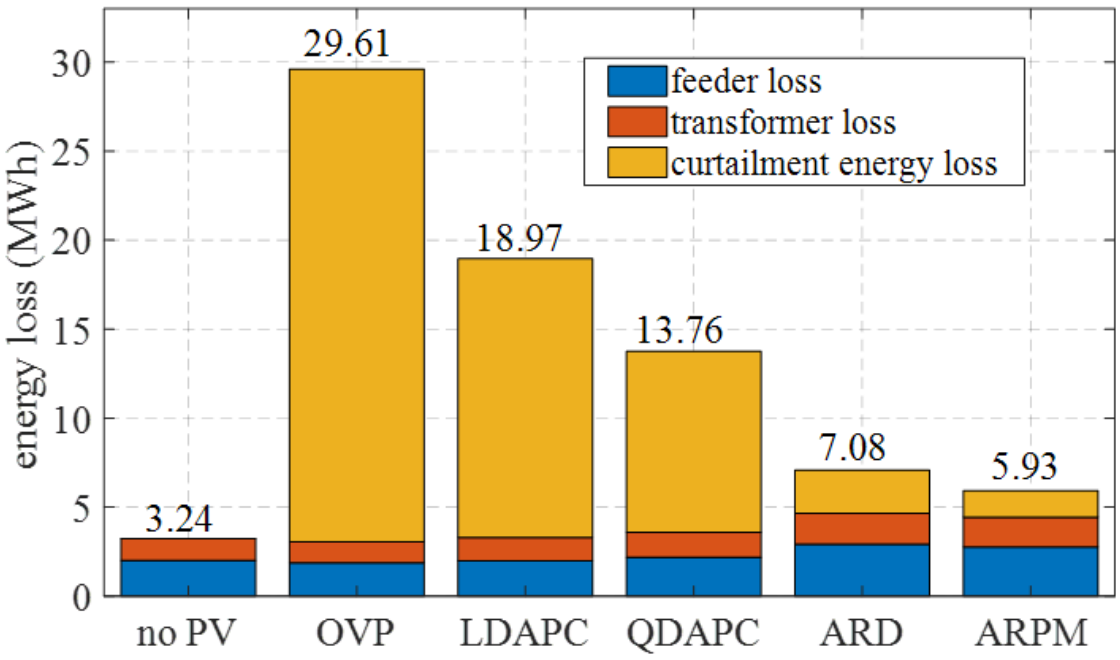

Figure 3.5. Comparison of energy loss between PV inverter controllers for the year 2014 compared to no PV case. The curtailment loss dominated feeder and transformer loss with controllers using only active power (OVP, LDAPC, QDAPC) and reverse is true for the controller using both active and reactive power for overvoltage protection (ARD, ARPM).

turn increases the distribution system losses. In other words, the distribution system losses are dependent on the amount of net power circulating in the feeder, which depends on the self-consumption of PV generation by the houses. However, these results cannot be generalized and might differ for different loading, irradiance data, and PV installation that were not considered in this paper. The idea is to provide a general idea of the behavior of each method.

3.2.4 Impact on Distribution Transformer Loading

The energy loss discussed in the previous section, along with reactive power absorbed in the feeder, is supplied by the distribution transformer, affecting the transformer loading. The impact of the different PV controllers on apparent power loading

of the distribution transformer is shown in Fig. 3.6 as a kernel density estimation. The figure shows how often the distribution transformer had a given loading (in kVA) throughout the annual simulation for each controller, compared to the no installed PV case.

With the addition of PV in the distribution system, the transformer at times is loaded near full capacity. Droop-based APC control methods loaded the transformer up to 60 kVA, at which point all active power would be curtailed based on voltages reaching the threshold. The larger density for higher apparent power loading with ARD and ARPM is due to reduced active power curtailment and increased reactive power absorption, indicating a higher chance of utilizing the transformer near full capacity. Analysis of the apparent power loading of the transformer is important to ensure that the transformer is not overloaded with an increasing PV installation. In addition, the results provide insight in areas where additional transformer loading (which increases temperature) can accelerate the degradation process of these units.

3.2.5 Financial Impact on Utility, Government, and End-users

The prior analysis presented the technical impacts of the inverter controllers. In this section, the long-term economic impact of overvoltage prevention inverter controllers is analyzed using two different pricing structures, specifically RTP and flat rate tariff. The deviation of energy consumption pattern based on the RTP (e.g., price-based demand response of the consumer) of end-user is not considered for the study.

The electricity tariff scheme has a significant impact on the financial benefit of the end-user, utility, and government. The electricity charges paid by the end-user can be split

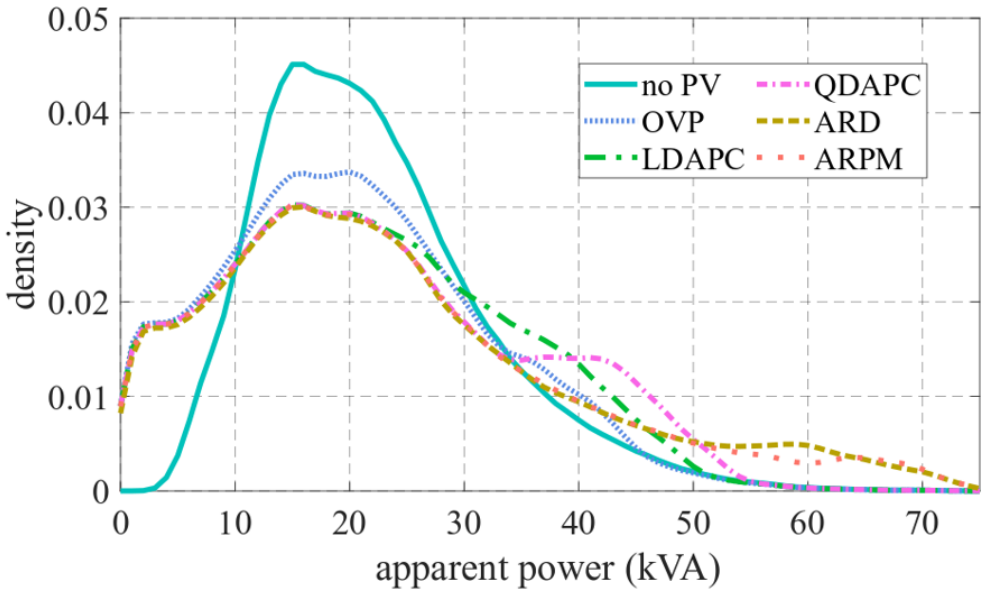

Figure 3.6. Kernel density estimation for an annual apparent power loading of 75 kVA transformer with different PV inverter controllers compared to no PV case for 2014. Transformer was lightly loaded with no PV, medium loaded with active power based controllers (OVP, LDAPC and QDAPC) and loaded close to full capacity with controllers using both active and reactive power (ARD, ARPM).

into three major categories: supply charges, distribution charges, and taxes and fees as described in Section 3.1.3. The electric utility (e.g., ComEd) revenue benefits from distribution charges paid by the end-user. Government and energy agencies get a direct benefit from taxes and fees that end-users pay for consuming the electricity. The supply charges are paid to the regional transmission organization (RTO)/independent system operator (ISO), e.g., PJM, which operates the wholesale electricity market. The aggregated annual electricity bill incurred from all 12 houses is shown in Fig. 3.7. Observation of nearly identical electricity bills for both the RTP and flat rate tariff schemes when there is no PV installation in the system hints that ComEd designed the RTP in such a way that the overall benefit gained by the utility remains almost unaffected whether the end-user chooses RTP or flat rate tariff (assuming the end-user does not change their consumption behavior in response to the price).

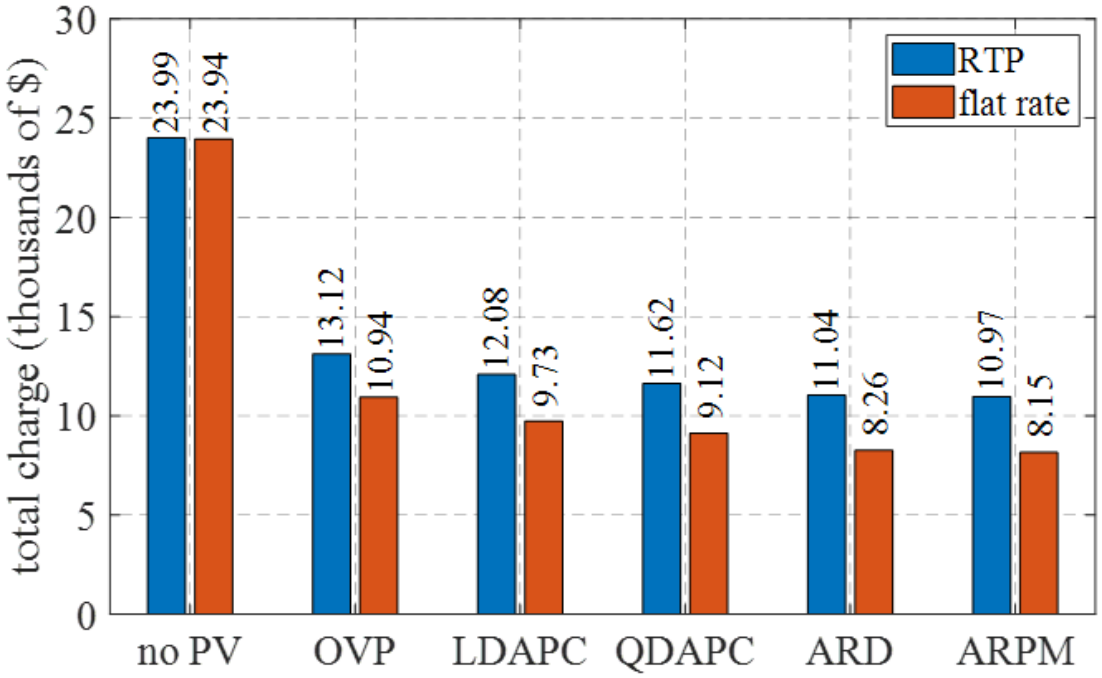

Figure 3.7. Comparison of total electricity charges paid by houses combined with two different tariff schemes- real time and fixed rate, compared among five different PV inverter controllers.

As the flat rate tariff is higher than RTP during peak PV generation, in general, the annual electricity bill is lower for end-users participating in the flat rate tariff. Because the total generation energy with 12 houses combined is in the increasing order OVP, LDPAC, QDAPC, ARD, and ARPM, the difference in total energy charges paid using two pricing schemes will increase in the same order.

As the different controllers directly impact the economic benefit of PV, the payback period of the PV installation is also impacted. Table 3.1 shows the payback period (computed by dividing the PV installation cost by the yearly income from PV, neglecting interest) for the nearest (H1) and farthest (H12) house from the transformer for the different PV control methods with RTP and flat rate tariff pricing schemes. The cost of 8.4 kW PV system installation is chosen to be \$3.22/W [39]. As the electricity bill of the flat

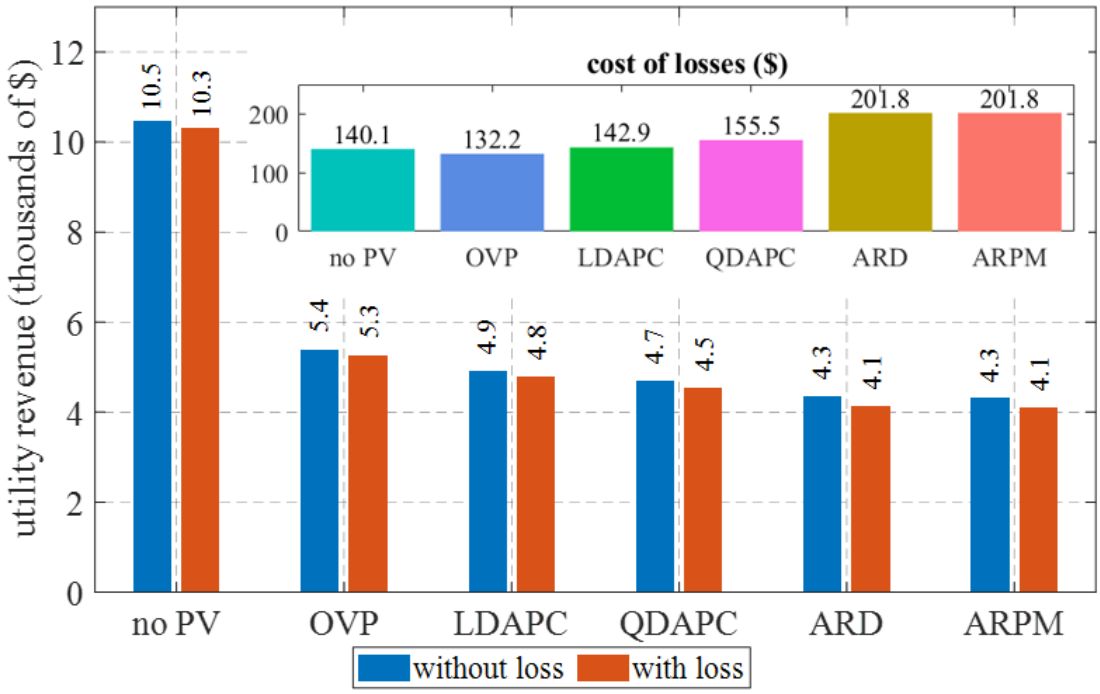

Figure 3.8. Utility benefit (electric sales minus energy purchased from ISO) with and without considering distribution system losses (higher is better for ComEd). The top-right box gives the cost of distribution system losses for the different types of PV inverter controllers.

rate tariff is lower as described above, the payback period will be shorter (when using net metering) regardless of the controllers for both houses. Similarly, since ARD and ARPM allow the inverters to inject more active power, the payback period will be reduced compared to the other three control methods, regardless of the type of tariff scheme adopted. For a given local control method (OVP, LDAPC, QDAPC, and ARD), because the nearest house (H1) can inject more energy than the farthest house (H12), H1 will have a shorter payback period than H12 for the same tariff scheme. However with ARPM, as every house curtails the same amount of active power, all houses will have similar payback periods (with variations coming from the different load).

Fig. 3.8 shows the net benefit to the electric utility considering distribution losses in orange, and neglecting distribution losses in blue.

Table 3.1. Payback period for different PV inverter controllers for the nearest (H1) and farthest (H12) house from the transformer

house	tariff scheme	payback period (years)				
		OVP	LD APC	QD APC	ARD	ARPM
H1	RTP	17.2	17.2	17.2	17.2	17.3
	flat rate	14.2	14.2	14.2	14.2	14.3
H12	RTP	26.3	22.1	20.1	17.97	17.3
	flat rate	22.7	19	17.1	15.17	14.4

The overlaid bar graph represents costs associated with losses in the distribution system and is to be paid by the utility. To compute the net benefit to the utility, delivery charges (from both RTP and flat rate) have been considered (note that both supply charges, and taxes and fees do not contribute to the utility benefit). As the utility has to pay for losses in the feeder and transformer, the net utility benefit is reduced when considering losses in all controller schemes. The net benefit gained decreased in the same order as the decreased energy consumption. The reduction in benefit is mainly caused by reduced total energy consumption due to the increased local power production using PV by the houses. The increased cost of losses from ARD and ARPM is due to higher reactive power absorption from PV houses to control the overvoltage (ultimately supplied by the distribution transformer).

To show the impact on government and agencies working for social benefit, the taxes and fees paid by the end-user is shown for different inverter controllers in Fig. 3.9 for the two pricing structures.

The annual aggregated taxes and fees paid by the 12 houses decreased in the same order as the utility benefits for both tariff schemes because of reduced energy consumption by end-users. Similarly, the total taxes and fees paid by the 12 houses are lower for RTP

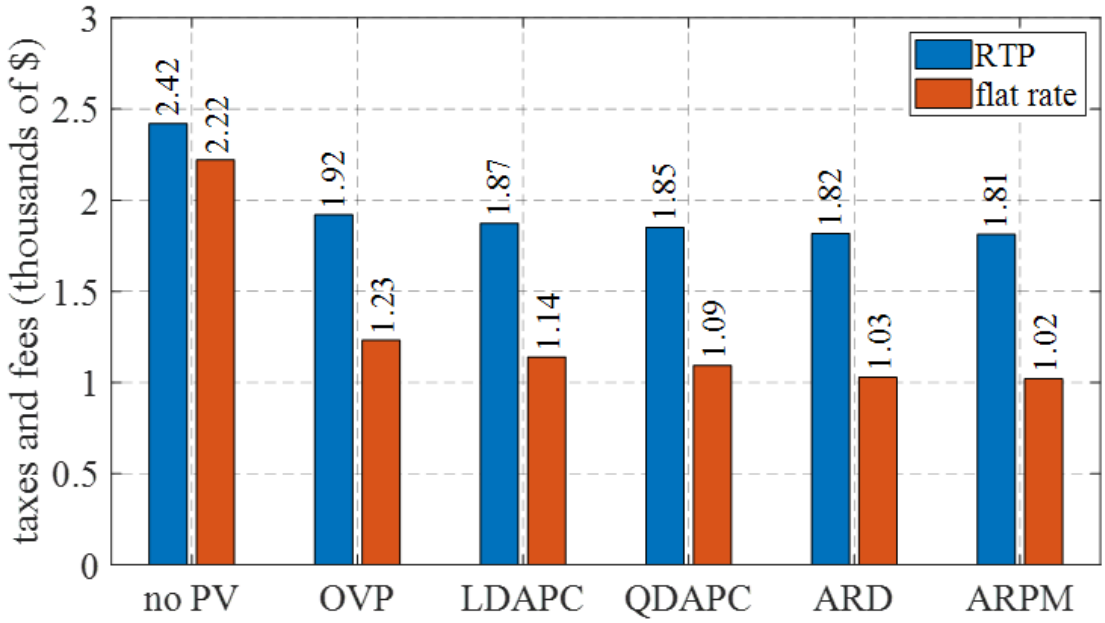

Figure 3.9. Total taxes and fees paid by all houses for different PV inverter controller for RTP and flat rate tariff.

compared to flat rate tariff because of the higher flat rate during high PV generation. The benefit to the government and utility *decreases* when using more effective (in a sense of lower total energy curtailment) inverter overvoltage prevention control methods. As the change in customer behavior has not been considered in this analysis for RTP, thus the results might not reflect all benefits to customers adjusting to this tariff.

CHAPTER 4 SUSTAINABILITY STUDY

4.1 Background and motivation

Sustainable development is defined as development that meets the needs of the present without compromising the ability of future generations to meet their needs by the World Commission on Environment and Development [40]. Sustainability has three pillars - social, economic and environment. For any technology to be sustainable it should be socially, economically and environmentally sustainable. Fig. 4.1 shows these three aspects of sustainability.

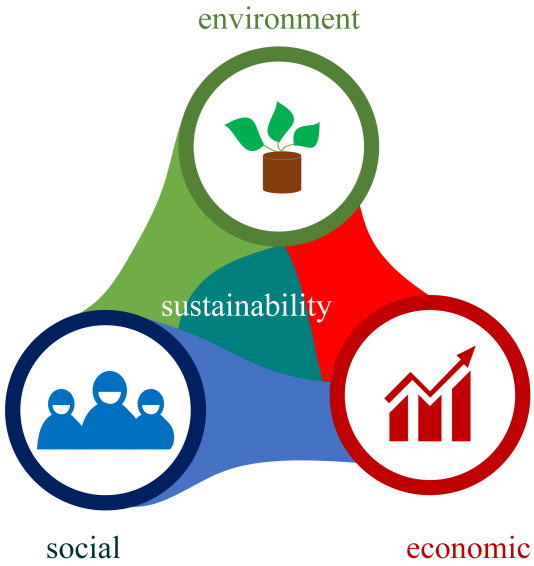

Figure 4.1. Three dimensions of sustainability- social, economic and environment.

4.2 Proposed Sustainability Metrics

The PV inverter can be controlled in a different fashion depending upon the implementation strategy to prevent overvoltage. Different types of inverter control strategy may have different social, economic and environmental impacts. It is important to

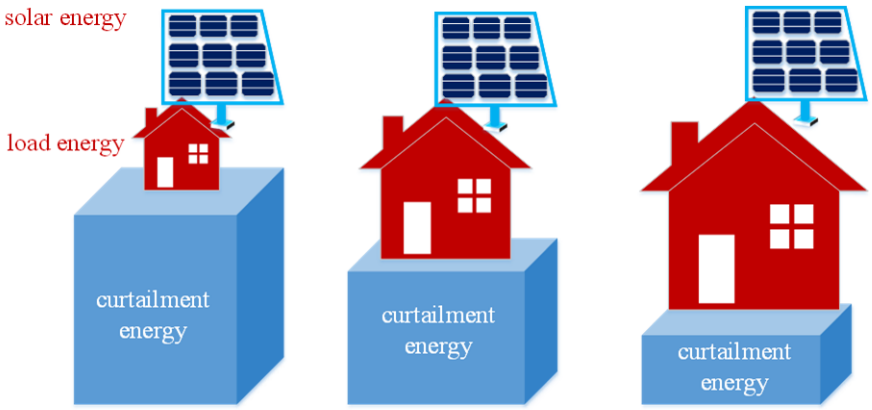

Figure 4.2. Fair curtailment between houses of a different generation and load. Size of the house in proportion to the electrical load. Same panel size indicates the same PV capacity on each house. House with the lower load will have a higher net generation so curtailment will be higher, as represented by the bigger cube.

quantify these impacts to select ideal control strategies and also compare the performance of existing control strategies. In this chapter, separate metrics are proposed to measure each of the sustainability and explained in detail below.

4.2.1 Social sustainability metric

Social sustainability is defined as the ability of a social system to indefinitely function at a specified level of social well-being and harmony. One aspect of social sustainability is social equity — the fair distribution of societal resources (e.g., jobs, local services) [41]. Fig. 4.2 is used to illustrate this concept which shows that house with higher net generation (solar generation subtracted from self-consumption) needs to curtail more to achieve the distribution of opportunity.

For differences due to network location, we define a loss of opportunity factor, μ_i, as the ratio of energy curtailed to the maximum possible energy injection of PV inverter i. At time t, let $p_{inv}^{i,t}$, $p_{mppt}^{i,t}$, and $p_l^{i,t}$ be the inverter active power output, maximum available

solar power, and active power demand, respectively. Over a time period T, μ_i is defined in (4.1).

$$\mu_i = \sum_{t=1}^{T} \frac{p_{mppt}^{i,t} - p_{inv}^{i,t}}{p_{mppt}^{i,t} - p_{l}^{i,t}} \tag{4.1}$$

Because $p_{mppt}^{i,t} \geq p_{inv}^{i,t}$, the numerator is non-negative. The denominator, however, can be positive, negative, or zero. A positive denominator means that the net energy produced by the PV is greater than the user's demand, which means the customer contributes to overvoltage. Overvoltage at a distribution node could also be due to higher neighborhood net generation, however, even when the user's PV generation is lower than their demand (i.e., μ_i is negative), which for some controllers means the user PV is curtailed even though they do not contribute to the overvoltage.

Ideally, μ_i for all PV units should be equal for a fair distribution of curtailment (i.e., equal opportunity to inject PV). However, depending on the PV inverter control strategy, feeder parameters, spatial location of PV units, and load profiles, μ_i may vary drastically between PV systems. For N PV inverters, let $\bar{\mu}$ be the mean loss of opportunity. A metric for social sustainability, η_{ssm}, can then be defined in terms of the root mean square difference of the loss of opportunity for all PV inverters defined by (4.2). When $\eta_{ssm} = 1$, all PV inverters have the same loss of opportunity, resulting in a fair overvoltage mitigation strategy. This concept can be extended to any type of distributed generation or energy program.

$$\eta_{ssm} = \frac{1}{1 + \sqrt{\frac{\sum(\mu_i - \bar{\mu})^2}{N}}} \tag{4.2}$$

4.2.2 Economic sustainability metric

Economic sustainability is related to the revenue earned, in this case, it quantifies how much revenue can be earned by installing PV on rooftop house. Fig. 4.3 shows that increasing PV installation should result in higher economic benefit to achieve economic sustainability.

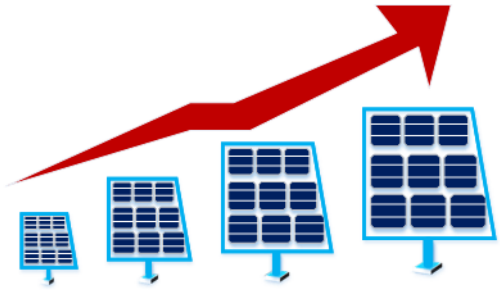

Figure 4.3. Increasing PV installation should provide higher economic revenue for economic sustainability

Determining economic sustainability metric requires knowledge of electricity tariff schemes. Utility buys electricity from the wholesale market whose price changes on an hourly basis in real market in US (e.g. PJM electricity market). Customers buy electricity at retail price, which could be a flat rate, could change in real time, or could be based on time of use.

(a) **Wholesale electricity tariff**

In an electricity market, the price of electricity at each node in transmission level changes in a regular interval of time (e.g. hourly basis) - often referred to as locational marginal price (LMPs). LMP at a particular transmission node is defined as the price of electricity to generate one more unit of electricity at that node. LMP

is obtained from the solution of optimal power flow – which is a non-linear optimization problem set up to minimize the total cost of electricity generation subject to power system constraints. In absence of line congestion LMP remains the same at all nodes, however, that is not always the case. Sometimes load in a particular area may be high enough that importing cheap electricity from other areas might become unfeasible due to line limit, and they may have to generate electricity using more expensive generating units increasing the price of electricity at that node. Ideally, utility (the entity that sales electricity to local customers) buys electricity at LMPs unless some small charges are added to cover up the cost of transmission infrastructure and other costs. The price at which utility buys electricity from the wholesale market is called wholesale electricity tariff.

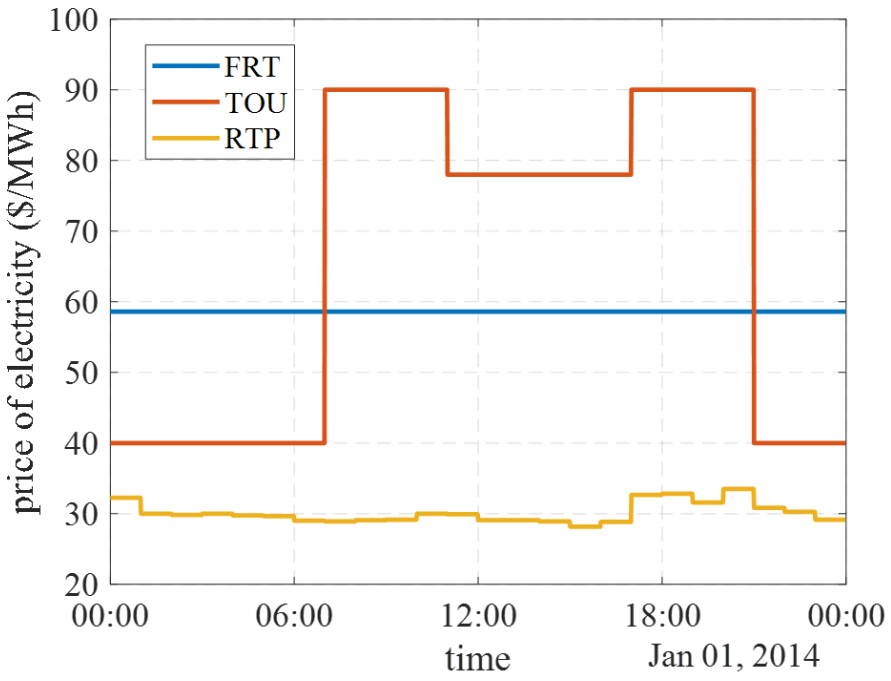

Figure 4.4. Three different retail tariff structures used for computing economic sustainability metrics - fixed rate tariff, time of use and real-time pricing.

(b) **Retail electricity tariff**

The price at which the consumer buys electricity is called retail electricity tariff. Three different types of retail electricity tariff schemes used for computing economic sustainability metrics are described below:

- *Fixed rate tariff (FRT):* In fixed rate tariff, customers buys energy at fixed price. In reality, utility adds other costs such as distribution charges, taxes, and other costs as well on top of actual energy cost.
- *Time of use (TOU):* In this tariff structure, price of electricity changes based on time of use. An example TOU tariff is shown in Fig. 4.4.
- *Real time pricing (RTP):* Electricity price changes in real-time in this tariff. An hourly real-time electricity tariff is shown in Fig. 4.4 along with TOU and FRT tariff.

When considering the economic well-being of residential PV, customer and utility well-being should be considered. In this study, we define an economic sustainability metric based on the net benefit to the consumer and utility of installing versus not-installing PV. At time t, let $p^t_{u,\text{no PV}}$ and $p^t_{u,\text{PV}}$ be the total active power supplied by the utility with and without PV, respectively, λ^t_{r} and λ^t_{w} be the retail and wholesale electricity prices, respectively, and Δt be the time-step. The economic sustainability metric can then be calculated as (4.3).

$$\eta_{esm} = \sum_{t=1}^{T} \left(\sum_{i=1}^{N} \left(p^{i,t}_{inv} \lambda^t_{\text{r}} \right) - \left(p^t_{u,\text{no-PV}} - p^t_{u,\text{PV}} \right) \lambda^t_{\text{w}} \right) \Delta t \tag{4.3}$$

The first term in the metric measures the customer benefit by summing revenue from all PV units based on the retail rate (e.g., real-time, fixed, time of use). The second term measures the potential economic loss for the utility as a reduction of electric sales caused by the installed PV. Revenue earned by consumers should be greater than the potential utility revenue loss in an economically sustainable system (i.e., $\eta_{esm} \geq 0$).

4.2.3 Environmental sustainability metric

Renewable energy generation reduces pollutant emissions from centralized fossil plants by replacing a portion of the generation with zero emission energy. Fig. 4.5 shows that emission should reduce with increasing PV installation to achieve environmental sustainability.

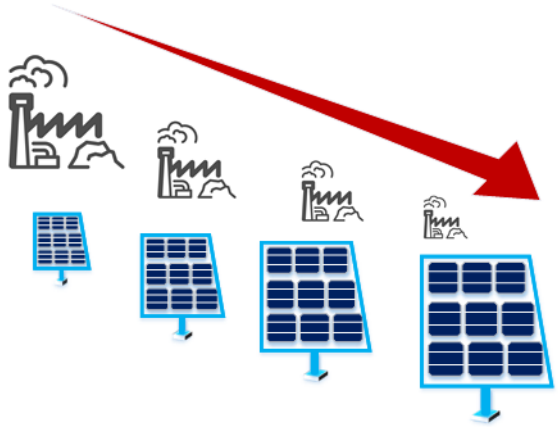

Figure 4.5. Increasing PV installation should reduce global emissions for environment sustainability.

The quantity of emission reduced depends on the generation supply mix of the power system, which varies through time, and the marginal generator. Having knowledge of emission reductions achieved by adopting certain technologies is beneficial in stakeholder decision making. In this study, the environmental sustainability metric is

defined as a percentage reduction in CO_2 emissions before and after installing the PV system under different PV inverter control strategies. Let $e_{\text{no PV}}$ and e_{PV} be the marginal on-peak CO_2 emission for a given period T with and without PV, respectively. At time t, let ω^t be marginal on-peak CO_2 emissions (in lbs./kW over time period Δt). The environmental sustainability metric for PV, η_{ensm} can then be calculated as:

$$\eta_{ensm} = \frac{e_{\text{no,PV}} - e_{\text{PV}}}{e_{\text{no,PV}}} = \frac{\sum_t (\sum_i p_{inv}^{i,t}) \omega^t}{\sum_t (\sum_i p_l^{i,t}) \omega^t} \tag{4.4}$$

4.3 Application of Sustainability Metrics

In this Section, we are going to compare the sustainability metrics for different PV inverter controllers explained in Chapter 2. The same set-up and parameters as provided in Chapter 3 are used for sustainability study. As ComEd did not provide information about the time of use (TOU) retail tariff, the price information for TOU is grabbed from Southern California Edison Website [42]. To make a fair comparison, average TOU price is made equal to the fixed rate tariff from ComEd. The real-time hourly LMPS (Locational Marginal Prices) is grabbed from PJM (a regional transmission organization in the U.S., that regulates wholesale electricity market) website [43] for the same year, and is used as a wholesale electricity price for utility in order to compute economic sustainability metric. PJM also publishes CO_2 emissions data (lbs/MWh) for marginal on peak unit. The emission data for the year 2014 is used to compute CO_2 emissions with and without PV for different PV inverter controllers based on the amount of monthly energy generation. The energy is assumed to be supplied to the distribution feeder always from the marginal on peak unit so that we could use PJM marginal on peak emission data from the same the

year to compute environmental sustainability metric.

4.3.1 Results and analysis

The social, economic, and environmental sustainability of the described inverter control methods were calculated and compared using the year-long simulation data. Fig. 4.6 compares the social sustainability metrics among the controllers. The droop-based methods that only used active power curtailment (LDAPC, QDAPC) for overvoltage prevention and the normal overvoltage prevention inverter control (OVP) show lower social sustainability.

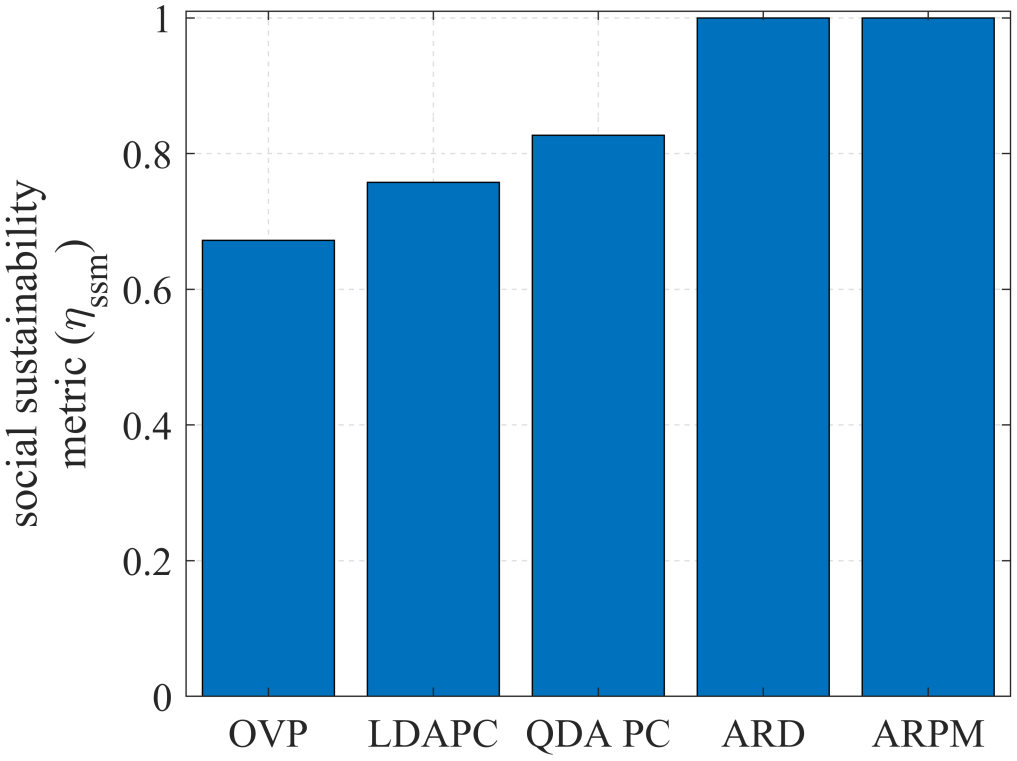

Figure 4.6. Social sustainability metrics of five different local PV inverter controllers. Higher value is preferred for higher sustainability.

The lower social sustainability is because houses near the substation never curtail,

whereas houses farther from the substation needed to curtail high amounts of energy to prevent overvoltage, leading to a loss of opportunity for those users far from the transformer. By using reactive power (i.e., ARD and ARPM), the need for active power curtailment significantly reduced, and the variation in loss of opportunity reduced, which significantly increased social sustainability. The use of a communication signal in ARPM allowed a slightly more fair distribution of loss of opportunity between houses, but the cost of the required communication infrastructure may not justify the increased fairness achieved.

Among the three tariffs, TOU provided the highest economic benefit and RTP provided the least in all simulated inverter control schemes, shown in Fig. 4.7. The

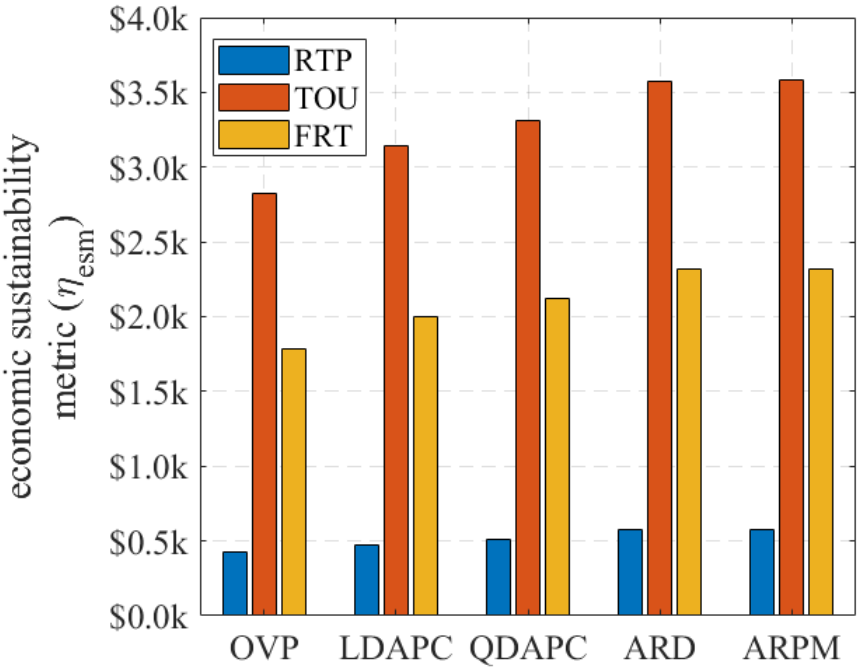

Figure 4.7. Economic sustainability metrics for five different local PV inverter controllers. Higher value is preferred for higher sustainability.

difference is because the peak PV output and RTP peak do not coincide, while during high

PV times the TOU price is high (i.e., shoulder and peak hours). Among the different inverter controllers, those that use reactive power (ARD, ARPM) injected more active power, resulting in higher economic revenue irrespective of the tariff schemes adopted.

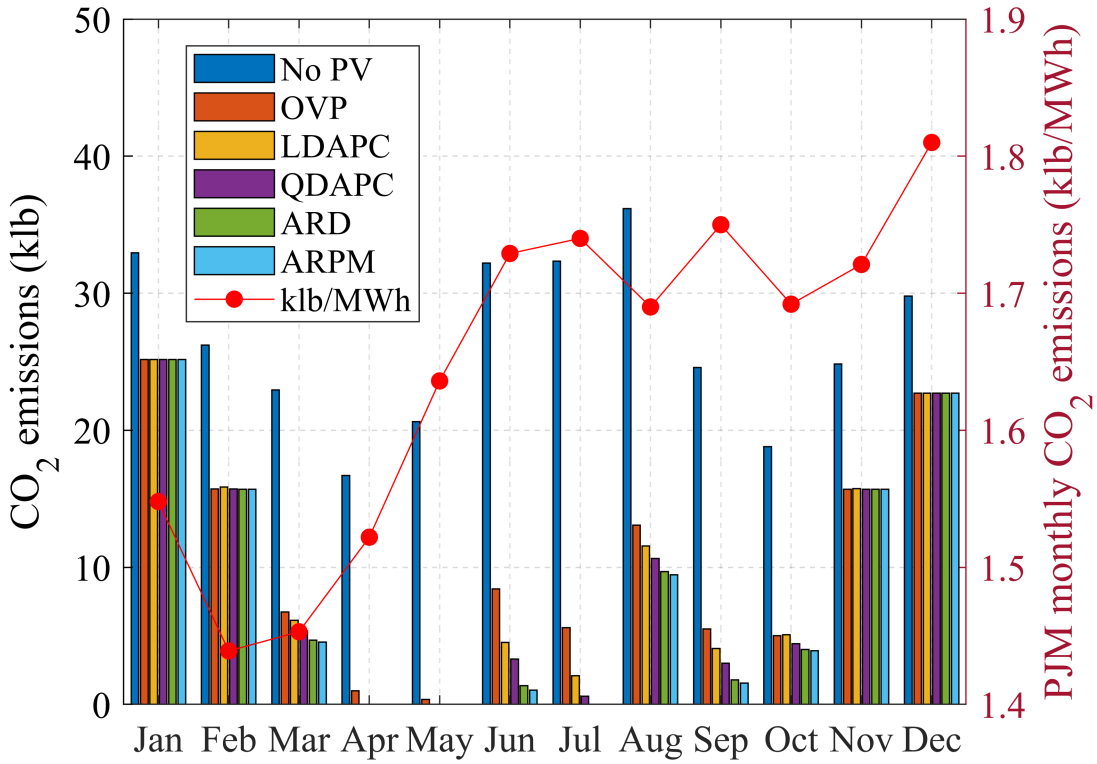

Figure 4.8. Monthly production of CO_2 in *lbs* for different PV inverter controllers based on PJM average emission data from 2014 compared to no PV case on the left. The solid red line on the right shows marginal CO_2 emission from PJM.

Fig. 4.8 shows the monthly CO_2 emissions for different PV inverter control schemes compared to No PV case on left vertical axis. The right vertical axis shows the monthly marginal on peak CO_2 emissions data from PJM for the year 2014. The emission was higher for the winter months, possibly due to higher energy consumption during these months, and could have been supplied using coal and/or natural gas peak power plants. During summer months, some PV inverter controller observed zero emission because

combined PV energy generation was higher than the combined energy consumption of the load.

To compute the environmental sustainability metric, the assumption is that every kWh produced by solar will replace the kWh from natural gas or coal power plants. Fig. 4.9 shows the variation of environmental sustainability metrics between different inverter control approaches.

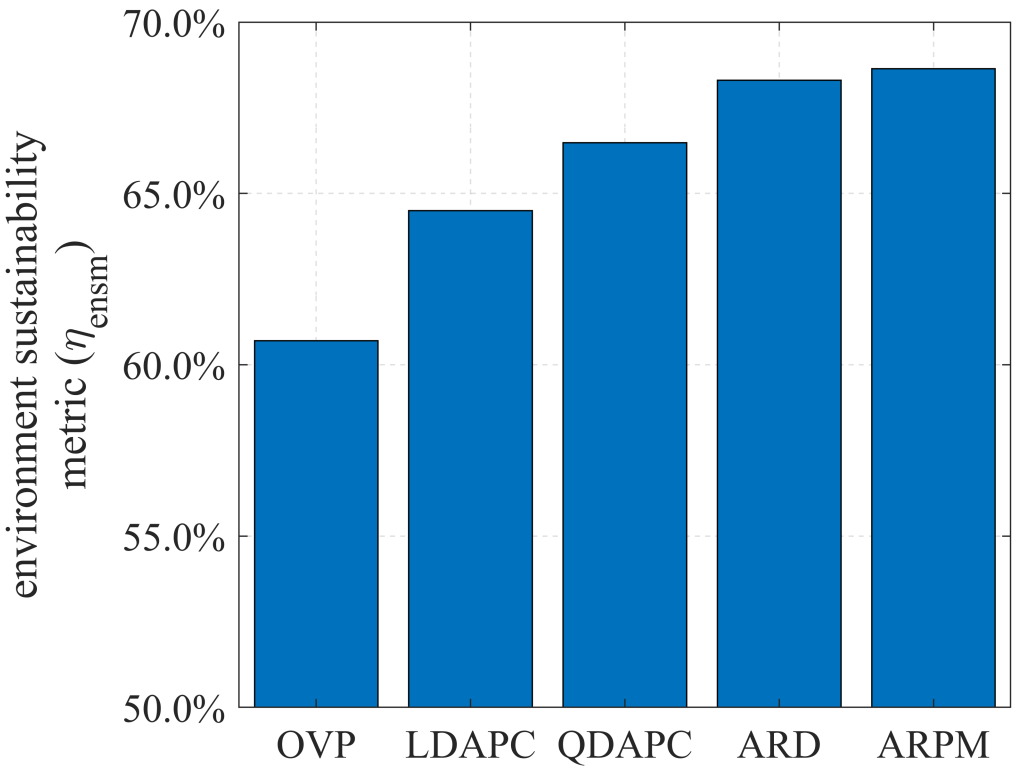

Figure 4.9. Environmental sustainability metrics for five different local PV inverter controllers. Higher value is preferred for higher sustainability.

These controllers that produced more energy proportionally reduced the emissions. The controllers absorbing reactive power (such as in ARPM and ARD) reduced emissions more than controlling using only active power curtailment (such as in OVP, LDAPC, and

QDAPC).

4.4 Multi-Objective Optimization

Generally, multi-objective optimization involves a set of conflicting objectives to explore trade-off. The found solutions are a set of Pareto-optimal solutions, where none are considered better than others. In this Chapter, linearized power flow equations are used to formulate multi-objective optimization to determine the trade-offs between the three sustainability metrics for PV overvoltage mitigation.

4.4.1 System description and optimization parameters

Consider a distribution network consisting of $N+1$ nodes collected in set $\mathscr{N} := 0,1,2,....,N$ and lines represented by the set of edges $\mathscr{E} := (m,n) \subset \mathscr{N} \times \mathscr{N}$ with Node 0 representing the secondary of the substation transformer. Subsets $\mathscr{N}^+, \mathscr{U}, \mathscr{H} \subset \mathscr{N}$ contain all nodes except node 0, nodes corresponding to utility poles, and nodes with connected PV, respectively. Note, utility poles neither inject nor absorb power.

At time t for all nodes in $\mathscr{N}^+$, let $\mathbf{v}^t$ be vector of voltage magnitudes, $\mathbf{p}^t_{inv}$ and $\mathbf{q}^t_{inv}$ be vectors of PV inverter active and reactive power respectively, and $\mathbf{p}^t_l$ and $\mathbf{q}^t_l$ be vectors of load active and reactive power, respectively. For nodes without PV, PV inverter active and reactive power are set to zero and for utility nodes, PV inverter power and load power are set to zero.

Similarly, $v^{i,t}, p^{i,t}_{inv}, q^{i,t}_{inv}, p^{i,t}_l, q^{i,t}_l, p^{i,t}_{mppt}$ denote the voltage magnitude, PV inverter active power, PV inverter reactive power, load active power, load reactive power, and maximum available power of i^{th} node at time t, respectively. For node without PV, $p^{i,t}_{mppt}$

is set to zero.

4.4.2 Linearized power flow equation

Power flow equations (meaning power inflow should be equal to power outflow at every node in the power system network) are highly nonlinear in nature which makes optimization problem hard to solve. Linear approximations of these power flow equations are proposed for radial network in [44], [45] given by equation (4.5). From these references, let $\mathbf{R} \in \mathbb{R}^{|\mathscr{N}^+|\times|\mathscr{N}^+|}$, $\mathbf{B} \in \mathbb{R}^{|\mathscr{N}^+|\times|\mathscr{N}^+|}$ and $\mathbf{a} \in \mathbb{R}^{|\mathscr{N}^+|\times 1}$ be network constants that depend on the admittance matrix (excluding slack bus), $\mathbf{Y} \in \mathbb{C}^{|\mathscr{N}^+|\times|\mathscr{N}^+|}$, and initial voltage magnitude. Power flow can then be linearized as (4.5).

$$\mathbf{v} = \mathbf{R}(\mathbf{p}_{inv} - \mathbf{p}_l) + \mathbf{B}(\mathbf{q}_{inv} - \mathbf{q}_l) + \mathbf{a} \tag{4.5}$$

Equation (4.5) shows that voltage magnitudes are linearly related to net injected active and reactive powers. No load voltage approximation was used to find **R**, **B**, and **a** of the network.

4.4.3 Multi-Objective Optimization Formulation

In this section, a multi-objective optimization problem is formulated based on maximizing social, economic, and environmental sustainability, subject to several technical constraints. Let $\mathscr{T} := 1, 2, ..., T$ be the set of time periods for the optimization. Eq. (5.3) ensures that the linearized power flow equations are satisfied.

$$\mathbf{v}^t = \mathbf{R}(\mathbf{p}^t_{inv} - \mathbf{p}^t_l) + \mathbf{B}(\mathbf{q}^t_{inv} - \mathbf{q}^t_l) + \mathbf{a}, \forall t \in \mathscr{T} \tag{4.6}$$

The voltage magnitude at all distribution nodes must be between the minimum (v_{min}) and maximum (v_{max}), given in (5.5).

$$v_{min} \leq v^{i,t} \leq v_{max} \forall i \in \mathscr{N}^+, \forall t \in \mathscr{T} \tag{4.7}$$

The reactive power of a PV inverter is limited by the allowed power factor. For a power factor angle ϕ, the reactive power output of a PV inverter is limited by (5.6).

$$|q^{i,t}_{inv}| \leq \tan(\cos^{-1}\phi) p^{i,t}_{inv}, \forall i \in \mathscr{H}, \forall t \in \mathscr{T} \tag{4.8}$$

The active power injection of the PV inverter must be between 0 and the maximum available power at that time for each node as given in (5.7).

$$0 \leq p^{i,t}_{inv} \leq p^{i,t}_{mppt}, \forall i \in \mathscr{H}, \forall t \in \mathscr{T} \tag{4.9}$$

The active and reactive power output of a PV inverter i must not exceed the inverter apparent power capacity, s^i_{inv}, given in (5.8).

$$\|(p^{i,t}_{inv}, q^{i,t}_{inv})\|_2 \leq s^i_{inv}, \forall i \in \mathscr{H}, \forall t \in \mathscr{T} \tag{4.10}$$

At utility nodes, the active and reactive load and active and reactive inverter power

must be set to zero at all times as formulated in (5.9) and (5.10).

$$p_{inv}^{i,t}, p_{l}^{i,t} = 0, \forall i \in \mathscr{U}, \forall t \in \mathscr{T} \tag{4.11}$$

$$q_{inv}^{i,t}, q_{l}^{i,t} = 0, \forall i \in \mathscr{U}, \forall t \in \mathscr{T} \tag{4.12}$$

The multi-objective optimization is then formulated as:

$$\max_{\mathbf{p}_{inv}^{t}, \mathbf{q}_{inv}^{t}, \mathbf{v}^{t}} \eta_{ssm}, \eta_{esm}, \eta_{ensm} \tag{4.13}$$

subject to (5.3)–(5.10).

4.4.4 NSGA-II for multi-objective optimization

To solve (5.11), we use the Non-dominated Sorting Genetic Algorithm II (NSGA-II) [46], provided by the *gamultiobj* function from MATLAB. NSGA-II maintains diversity in the population by choosing individual solutions even if they have lower fitness values, which is useful to converge to an optimal Pareto front. The algorithm starts with an initial population of feasible solutions (each individual solution is called a chromosome). Some of the terminologies used while implementing a genetic algorithm are explained briefly below.

- Rank: Each individual in a population is given a rank based on their fitness value using the iterative process. Individuals present in rank 1 are not dominated by other individuals, individuals present in rank 2 are dominated by individuals present in rank 1 and goes on. Individuals with lower rank have higher chances of selection.

- Crowding distance: A measure of closeness of an individual to it's nearest neighbors within the same rank. The distance can be measured in objective function space or decision variable space but default objective function space is used in this study. It is computed as the sum over the dimensions (indexed by m) of normalized absolute distance between sorted nearest neighbors. Individuals within the same rank with higher crowding distance have higher chances of selection.

- Spread: Measures the movement of Pareto set. Iterations stop when the spread does not change much, and the final spread is less than an average of recent spreads.

The genetic algorithm follows the following steps in each iteration.

Step 1: Parent chromosomes are selected from among the individual solutions based on some selection function (default binary tournament function could be any function customized)

Step 2: Children chromosomes are created using crossover and mutation

Step 3: Compute the score for each child based on objective function value and their feasibility

Step 4: Computing rank and crowding distance of each individual in an extended population (children and current population)

Step 5: Trimming of an extended population by retaining the appropriate number of individuals in each rank

The algorithm stops whenever the geometric value of the relative change in the value of spread is less than tolerance or number of generations exceed the maximum allowed generations or time limit exceeds.

4.4.5 Optimization Setup

The same distribution benchmark system previously used for comparing sustainability metrics between different PV inverter controllers is used to perform multi-objective optimization. To perform multi-objective optimization the highest irradiance of the same year 2014 is considered in an hour resolution because of the computation limitation of CPU to handle big size matrix (for minute resolution even for a day the size of matrix GA need to handle was 10 GB).

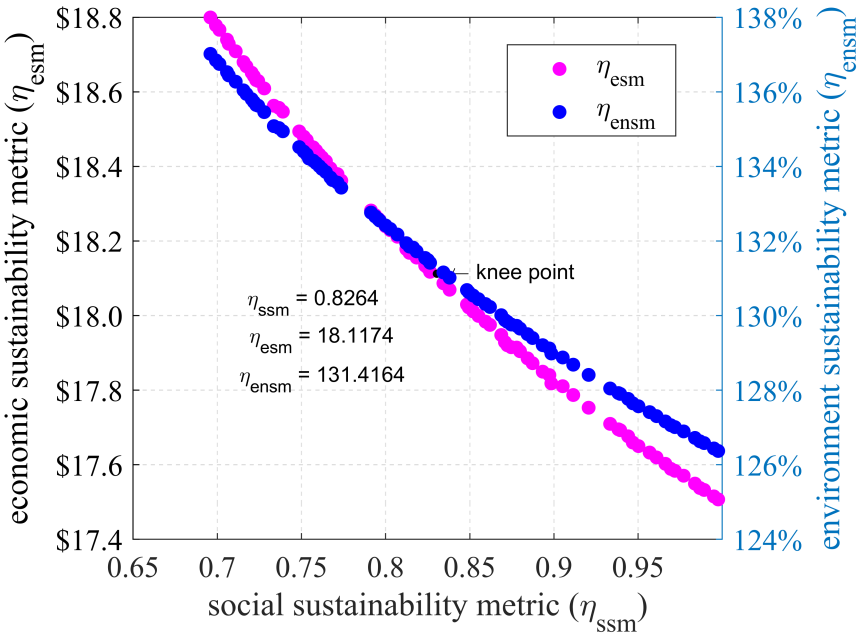

Figure 4.10. Pareto front obtained after performing multi-objective optimization consisting of 70 non-dominated solutions. Economic and environmental sustainability metrics on left and right are negatively correlated to social sustainability metric.

The solar and load data and how they are obtained already explained in the previous

chapter. Unity power factor is used to capture the worst case scenario which will result in maximum curtailment for implementation. To generate initial population random linear objective functions are optimized subject to same constraints, (5.3)–(5.10). In addition, individual solutions obtained by optimizing each sustainability metrics are also added in the pool of initial population to reach accurate solution set.

4.4.6 Result and analysis

Fig. 4.10 shows the Pareto front between the three sustainability metrics. Maximizing environmental and economic sustainability metrics were found to not be conflicting objectives because increasing economic sustainability was caused by increased active power injection, which corresponds to an increased reduction in CO_2 emissions.

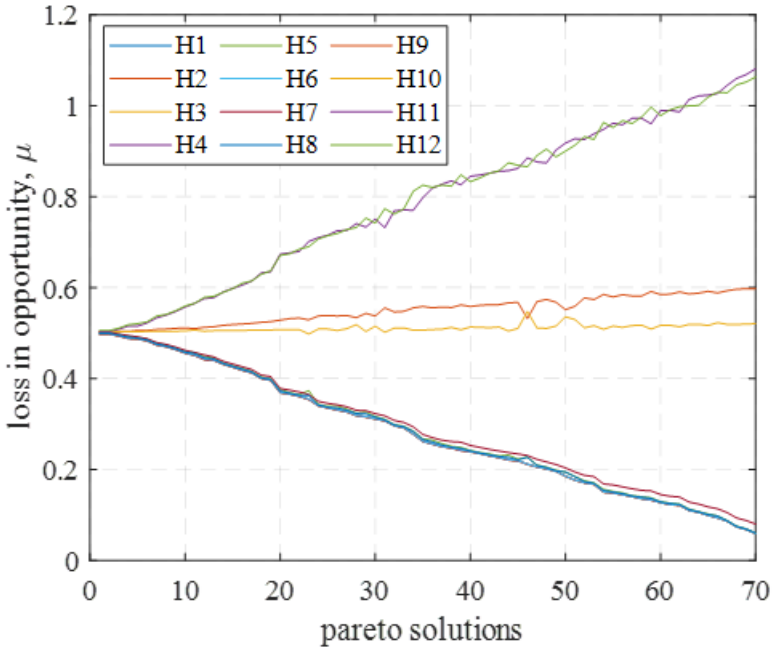

Figure 4.11. Variation in loss of opportunity factors between houses in different non-dominated solutions obtained after performing multi-objective optimization.

However, maximizing social sustainability metric directly opposes economic and environmental sustainability. If both objectives are equally important and a knee-point

exists on the Pareto front, this point would provide the best compromise, indicated by the curve's local maximum. To see how each Pareto solution evolved, we looked at the variation of loss of opportunity between the twelve houses. Fig. 4.11 shows that for Pareto solutions with higher social sustainability (left side of figure), a lower deviation in loss of opportunity between houses is observed.

As the solutions move toward more economic (or environmental) sustainability, the variation of μ_i between houses increased drastically. For the houses near the transformer (H1–H6) μ_i decreased, houses in the middle (H9, H10) μ_i remained almost same, and for the farther houses (H11, H12) μ_i dramatically increased. The variation in μ_i occurs because to achieve higher overall economic benefits, curtailment is high for houses situated farther from the substation compared to the nearer houses.

CHAPTER 5 ADDITIONAL STUDY ON HIGH PV PENETRATION

Apart from techno-economic and sustainability study of PV inverter controllers, I also worked on the marginal cost of distribution ancillary services and PV hosting capacity analysis which are also the major issues of increasing PV installation. The distribution system is limited in terms of the amount of PV that can be installed without needing further grid investments. Hosting capacity analysis helps to estimate the current potential of the distribution system. When the PV installed is more than the hosting capacity, distribution ancillary services such as active power curtailment, reactive power absorption may become necessary to maintain reliable distribution system operation. Having knowledge of the locational marginal cost of such services helps to provide an incentive to corresponding entities. At some point, depending on how far the current PV penetration is from hosting capacity, other grid investment along with PV inverter control may become the cost-effective solution.

5.1 Marginal Cost of Distribution Ancillary Services

The inverter can either absorb reactive power and/or curtail active power to mitigate overvoltage caused by increasing PV installation in the distribution feeder. Curtailment of active power reduces the economic benefit of having PV in the system and is not desirable. Absorbing reactive power reduces the need for active power curtailment for overvoltage mitigation indirectly increasing economic benefit. Note that, reactive power absorption might require higher inverter capacity, increase feeder loss however the motivation is that economic benefit of reduced curtailment exceeds other negative impacts. Any PV unit present in the distribution system can provide these ancillary services however some

nodes can be more effective than others. The major question is how can we assign the price for these services. Distribution optimal power flow is formulated in this thesis paper to find out the marginal cost of these services. A marginal active power curtailment cost, $\sigma_{i,APC}$, is the cost of curtailing next watt of power at i^{th} node. Similarly, a marginal cost for reactive power absorption, $\sigma_{i,RPC}$ for i^{th} node is defined. They can be used to provide incentives to PV units providing these services. σ_{APC} and σ_{RPC} are vectors collecting marginal costs from all nodes in the distribution network.

5.1.1 Distribution optimal power flow formulation

In this section, a distributed optimal power flow problem is formulated to determine the marginal cost of active power curtailment and reactive power absorption, subject to several technical constraints. Let $\mathbf{p}_{curt}$ and $\mathbf{q}_{absorb}$ be the vector collecting active power curtailment and reactive power absorption from all nodes in the distribution network defined in (5.1) and (5.2).

$$\mathbf{p}_{curt} = \mathbf{p}_{mppt} - \mathbf{p}_{inv} \tag{5.1}$$

$$\mathbf{q}_{absorb} = -\mathbf{q}_{inv} \tag{5.2}$$

For i^{th} node, p^i_{curt}, q^i_{absorb} are corresponding active power curtailment and reactive power absorption respectively. Note for utility nodes (node with no load and no generation) $p^i_{curt} = 0$ and $q^i_{absorb} = 0$. Equation (5.3) ensures that the linearized power flow equations are satisfied and is a modified version of the linearized power flow equation described previously.

$$\sigma_{APC} : \mathbf{p}_{curt} = \mathbf{R}^{-1}(\mathbf{R}(\mathbf{p}_{mppt} - \mathbf{p}_l) - \mathbf{B}(\mathbf{q}_{absorb} + \mathbf{q}_l) + \mathbf{a}) \tag{5.3}$$

Note σ_{APC} is just a vector of Lagrangian multipliers for the constraint vector defined in (5.3). These Lagrangian multipliers are essentially marginal costs - depending on how objective function is defined. Similarly to find out σ_{RPC} they can be written as in (5.4).

$$\sigma_{RPC} : \mathbf{q}_{absorb} = \mathbf{B}^{-1}(\mathbf{R}(\mathbf{p}_{mppt} - \mathbf{p}_{curt} - \mathbf{p}_l) - \mathbf{B}(\mathbf{q}_l) + \mathbf{a}) \tag{5.4}$$

The voltage magnitude at all distribution nodes must be between the minimum (v_{min}) and maximum (v_{max}), given in (5.5).

$$v_{min} \leq v^i \leq v_{max} \forall i \in \mathscr{N}^+ \tag{5.5}$$

The reactive power absorption of a PV inverter is limited by the allowed power factor. For a power factor angle ϕ, the reactive power absorption of a PV inverter is limited by (5.6).

$$|q^i_{absorb}| \leq \tan(\cos^{-1}\phi)(p^i_{mppt} - p^i_{curt}), \forall i \in \mathscr{H} \tag{5.6}$$

The active power curtailment must be between 0 and the maximum available power at that time for each node as given in (5.7).

$$0 \leq p^i_{curt} \leq p^i_{mppt}, \forall i \in \mathscr{H} \tag{5.7}$$

The active and reactive power output of a PV inverter i must not exceed the inverter

apparent power capacity, s^i_{inv}, given in (5.8).

$$\|(p^i_{mppt} - p^i_{curt}, q^i_{absorb})\|_2 \leq s^i_{inv}, \forall i \in \mathscr{H} \tag{5.8}$$

At utility nodes, the active and reactive load, and active power curtailment and reactive power absorption of inverter must be set to zero as formulated in (5.9) and (5.10).

$$p^i_{curt}, p^i_l = 0, \forall i \in \mathscr{U} \tag{5.9}$$

$$q^i_{absorb}, q^i_l = 0, \forall i \in \mathscr{U} \tag{5.10}$$

The objective is to minimize the cost of curtailment. If λ_{PV} is the levelized cost of PV energy (expressed either in cents/kWh or $/kWh) the objective can be formulated as in (5.11).

$$\min_{\mathbf{p}_{curt}, \mathbf{q}_{absorb}, \mathbf{v}} \sum_i \lambda_{PV} p^i_{curt} \Delta t \tag{5.11}$$

subject to (5.3)–(5.10).

Here, Δt is time interval (in an hour) for updating the marginal cost of active power curtailment and reactive power absorption in the market.

5.1.2 Levelized cost of PV

The levelized cost of the PV system (LCPV) is defined as the ratio of the total cost for installing and operating PV system to total energy produced over its lifetime.

$$\text{LCPV} = \lambda_{PV} = \frac{\text{life time cost of PV system}}{\text{lime time energy generation}} \tag{5.12}$$

The life time cost of PV system can be divided into five categories: development/planning (C_{dev}), PV panels (C_{Panel}), electrical apparatus ($C_{Elec.}$), mounting structure and civil work (C_{Civil}), in addition to operation and maintenance ($C_{O\&M}$) [47].

$$\text{LCC} = C_{dev} + C_{Panel} + C_{Elec.} + C_{Civil} + C_{O\&M} \tag{5.13}$$

Development and planning cost include research and development cost (such as grid impact study, environmental study), legal cost of permitting, cost related to finance or lease and land cost. Similarly, PV panel cost would include the cost of manufacturing solar panel (such as the cost of materials, assembling, smelting, wafering, etc.). Cost of physical installation such as labor cost, the construction set up, civil work, etc. comes under the mounting structure and civil work cost. Cost of inverters, wires, protection system, transformers, interconnection to AC grid, etc. comes under electrical cost. Operation and maintenance cost includes the cost of component replacement and labor for operating PV system if needed.

Equation (5.12) is more general definition. We used installation cost ($2.8/kW), inverter replacement cost (0.13/kW), degradation factor of PV panel (0.75%) and inflation rate (2.5%) for residential PV system from [48] to compute λ_{PV} of 8.4 kW PV system considered in this study. The Payback period of 10 years is considered for this study. The λ_{PV} for 8.4 kW is found to be 21.44 cents/kWh. The solar data is taken from [36] to compute estimated available energy generation ($\approx$118 MWh considering 0.75%

degradation rate and 10 years payback period).

5.1.3 Set-up for distribution optimal power flow

The same 12 house radial distribution feeder (description available in chapter 3) is used to compute the marginal cost of active power curtailment and reactive power absorption in 10-minute resolution for the highest irradiance day (June 22, 2014). Load data and solar data are the same as used in previous chapters. For each time, the optimization is solved independently (no time coupling constraints) using Optimization Toolbox in MATLAB.

5.1.4 Marginal cost of active power curtailment

The marginal cost of active power curtailment (cents/kW) for the next 10 minute at various distance from the substation is shown in Fig. 5.1. The cost is zero when there is zero curtailment (no overvoltage occurs). The curtailment happens during an afternoon when solar power is available (when overvoltage occurs and curtailment is used to mitigate overvoltage) and curtailment price becomes nonzero. The marginal cost of curtailment increased with increase in distance from substation where PV is installed. The increment in marginal cost is because the same curtailment can cause higher voltage change with an increase in distance.

5.1.5 Marginal cost of reactive power absorption

The marginal cost of reactive power absorption (cents/kVAR) for the next 10-minute at various distance from the substation is shown in Fig. 5.2. The nonzero curtailment price appears whenever curtailment occurs to prevent overvoltage. The reactive power absorption does not directly cost money; however, it helps to reduce the need for active

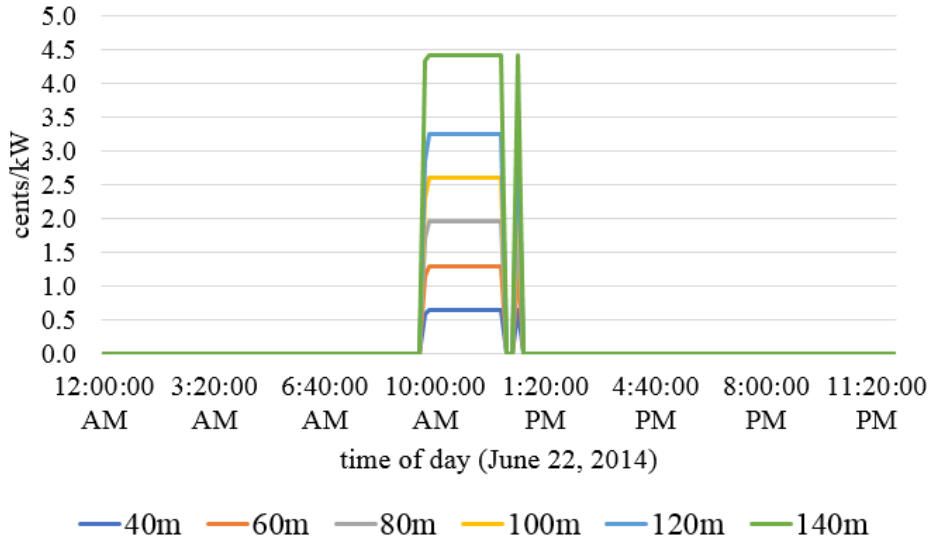

Figure 5.1. Marginal cost of active power curtailment in 10 minute resolution at various distances from distribution substation for June 22, 2014.

Table 5.1. Incentives for active power curtailment and reactive power absorption

House	active power curtailment incentive (cents)	reactive power absorption incentive (cents)
H1, H2 (40m)	0.0, 0.0	62.27, 62.27
H3, H4 (60m)	0.0, 0.0	68.8, 68.8
H5, H6 (80m)	0.0, 0.0	7.32, 75.32
H7, H8 (100m)	0.0, 0.0	81.84, 81.84
H9, H10 (120m)	0.0, 0.0	88.36 88.36
H11, H12 (140m)	108.1, 105.5	80.09, 79.63

power curtailment. And incentive should be provided to those units which are providing these services.

The marginal cost of reactive power absorption increased with increase in distance from substation where PV is installed. The increase in marginal cost for reactive power absorption is because the same reactive power absorption can cause higher voltage change with an increase in distance. The marginal cost of reactive power absorption is less than the marginal cost of active power curtailment because active power is more sensitive to voltage change than reactive power.

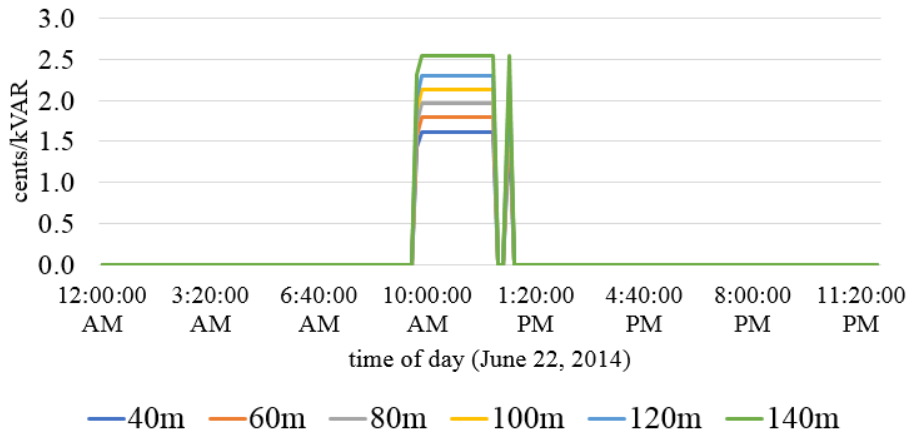

Figure 5.2. Marginal cost of reactive power absorption in 10-minute resolution at various distances from distribution substation for June 22, 2014.

5.1.6 Total cost of services

Table 5.1 shows how much each house would receive for providing active power curtailment and reactive power absorption service as an incentive. Total incentives for active power curtailment is $2.05 and for reactive power absorption $9.46 should be paid because of the higher quantity of reactive power absorption (0.95 leading and lagging power factor limit) compared to the quantity of active power curtailment needed to prevent overvoltage. The total cost of incentive would be $10.5 for a day. The cost would increase to $16 if reactive power is not allowed to be absorbed by an inverter for voltage regulation.

5.1.7 Summary of Study

The concept of the locational marginal cost of ancillary services (such as active power curtailment and reactive power absorption) provided by the PV inverter for voltage mitigation studied in this research work can help utilities to provide incentives for such services.

5.2 Monte-Carlo based PV hosting Capacity Analysis

PV power generation is highly variable in nature and poses several challenges while integrating with the electric grid. The main factor that prevents PV installation is overvoltage, which limits the PV hosting capacity of the feeder [23]. Several studies were performed in the past few years to understand the impact of PV penetration in a distribution feeder. Ultimately, PV integration challenges limit the installation of PV in a feeder. Integrating more PV than the feeder hosting capacity requires a distribution system or PV inverter control upgrades. The distribution system hosting capacity upgrade costs vary significantly with PV penetration level, and the cost is dependent on size and spatial location of PV in the feeder [49]. As the location, size and orientation of the PV installations along with load profile in a particular feeder are random in nature, Monte Carlo simulation is a common approach for such a study. High penetration PV case studies were conducted for a 1.2 MW plant in Kaua'i Island Utility Cooperative, Hawaii, and a 2 MW Plant in Fontana, California. These preliminary results suggest that utilities could install very high levels of PV in localized areas without causing reverse power flow conditions at the substation [50].

A key factor in capturing different voltage issues is the simulation timestep. The voltage fluctuations caused by short-term solar power fluctuations cannot be addressed by a large resolution, long-term study in [51]. To capture such behavior requires using a smaller resolution (i.e., smaller simulation timestep), necessitating more computation. Moreover, with increasing PV penetration level, their effect on medium voltage and high voltage transmission networks also becomes significant, increasing the required network

size to be simulated. The inclusion of cloud movement data, weather data, and locational and seasonal variations in power output of PV installation additionally increase the computation burden. The need for computation increases even more with an increase in possible scenarios to be run for different levels of PV penetration. The size of the Monte Carlo analysis grows rapidly as the number of scenarios, system size, and time duration for study increases. Running a large number of DG (e.g., PV) scenarios for longer time periods helps to better design and operate the distribution system. Evaluation and analysis of different PV penetration scenarios are highly stochastic and repetitive in nature. Linear complexity and high scalability of a Monte Carlo method are favorable for parallelism. In [52], a comparison is made between implementations of Monte Carlo using OpenMP or CUDA for an identified problem in a system of 10 million particles. In [53], graphics processing units (GPU) is used to increase the speed of Monte Carlo simulations.

5.2.1 Methodology

To perform a Monte Carlo analysis, different randomly generated PV penetration scenarios are created. The PV penetration (defined as the percentage of houses having PV compared to the total number of houses) is varied from 10% to 100% in 10% increments, with 25 scenarios per penetration level (except for 100%). Each scenario is created by randomly selecting the location of PV units to be connected to the system. The load data and solar irradiance data does not change between scenarios. The location and size of the installed PV at each node are the random variables in each of the scenarios. In total, 251 Monte Carlo scenarios are simulated. Because each scenario is independent, the scenarios can be distributed to separate processing elements in an HPC to reduce the total

computation time of the study.

The parallel algorithm was developed in Python and run on the “Roaring Thunder” cluster at South Dakota State University (SDSU). Roaring Thunder has 56 compute nodes (2 CPUs with 20 cores each, 192 GB RAM), 5 big memory nodes (4 CPUs with 20 cores each, 3 TB RAM), 4 GPU nodes (each with two NVIDIA P100 or T100 GPUs), and a 450 TB parallel file system connected via 100 Gbps Infiniband. Each parallel process randomly selects the location of PV panels in the distribution feeder based on the scenario penetration level, and input files are automatically generated. The input files are in “player file” format containing information about node net power injection — the difference between electric load and PV generation — at each simulation timestep. The player file is used by the distribution simulation software, GridLAB-D [33], to change node power at each timestep and run power flow. The voltage measurements are aggregated from each scenario to generate the plots in results section later. The workflow diagram to perform PV hosting capacity analysis is presented in Fig. 5.3.

The simulation for each PV penetration scenario is conducted for two days — the highest annual irradiance day and lowest annual load day. These days were chosen because we wanted to observe the effect on hosting capacity of distribution feeders for both cases which should correlate to the days with the highest PV impacts. The description of the distribution system benchmark and the solar and load power input data are explained in the next substation.

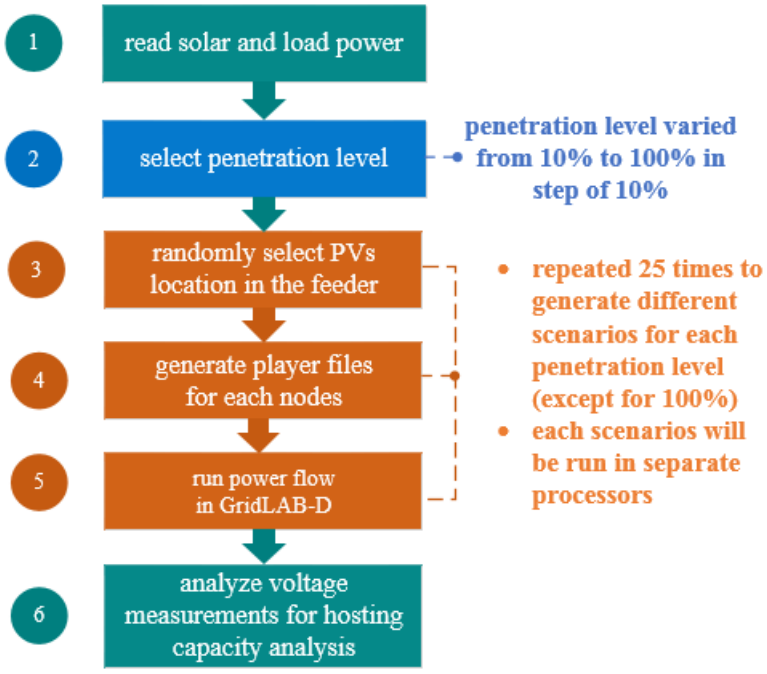

Figure 5.3. Flow diagram for performing PV hosting capacity analysis in a distribution feeder using high-performance computing.

5.2.2 Benchmark system

A Pacific Northwest National Laboratory (PNNL) taxonomy feeder R1-12.47-1 is selected for performing hosting capacity analysis in this paper, representing a moderately populated suburban and rural area of the western U.S. [54]. The voltage level is 12.5 kV for this feeder and the feeder model was developed in GridLAB-D[3]. A schematic of benchmark under consideration is presented in Fig. 5.4 [55].

5.2.3 Solar power data

To calculate the available PV power at each time interval, global horizontal irradiance (GHI) data was obtained from SolarAnywhere [36]. GHI is the total shortwave

[3]The feeder input in GridLAB-D format was taken from the Github repository available at `https://github.com/gridlab-d/Taxonomy_Feeders`.

Figure 5.4. Schematic of PNNL taxonomy feeder R1-12.47-1 used for hosting capacity analysis [55].

radiation obtained by a surface horizontal to the ground. The solar irradiance data is also taken from the western part of US to comply with feeder location. The available hourly solar irradiance data are converted to a one-minute resolution using linear interpolation. Each node in the benchmark taxonomy feeder with non-zero load values are considered as potential node points where residential PV can be connected. The amount of residential PV that can be connected at these node points was computed using 6 kW as the average PV installation size in US [56]. The location of the PV installations was uniformly randomly chosen based on each given penetration level. In this study, the effect of panel orientation is ignored and the same irradiance level is assumed for all PV panels. This assumption is conservative, as the hosting capacity of a feeder with these assumptions will be slightly less than actual.

Let η be the efficiency of the PV panel, I be the solar irradiance in W/m^2, and A be the area of the PV panel in m^2. Irradiance data is then used to calculate the maximum power available in the PV array (P_{MPPT}) as:

$$P_{MPPT} = \eta \times I \times A. \tag{5.14}$$

For a PV panel of 6 kW capacity, the efficiency is taken as 21.5% [57] and an area of 36.7896 m^2 [58].

5.2.4 Load data

To match the feeder and solar data location, hourly resolution load data from the California Independent System Operator (CAISO) is used [59]. The CAISO load data is also converted into a one-minute resolution using linear interpolation. The load is scaled to match the size of the taxonomy feeder derived from [35]. Let $l_{sys}(t)$ be the original system load, which in this case is the one-minute resolution CAISO load data. The scaling factor at a given time t, defined as $S(t)$, is then calculated as

$$S(t) = \frac{l_{sys}(t) - \min\limits_{t} l_{sys}(t)}{\max\limits_{t} l_{sys}(t) - \min\limits_{t} l_{sys}(t)}. \tag{5.15}$$

This scaling factor is then used in (5.16) to generate a time-varying load pattern at node point. For a given node point n_p, let $l(n_p,t)$ be the load data at time t, and $l_{min}(n_p)$ and $l_{max}(n_p)$ be 30% and 100% of the base load of the feeder model, respectively.

$$l(n_p,t) = l_{min}(n_p) + S(t) \times (l_{max}(n_p) - l_{min}(n_p)) \tag{5.16}$$

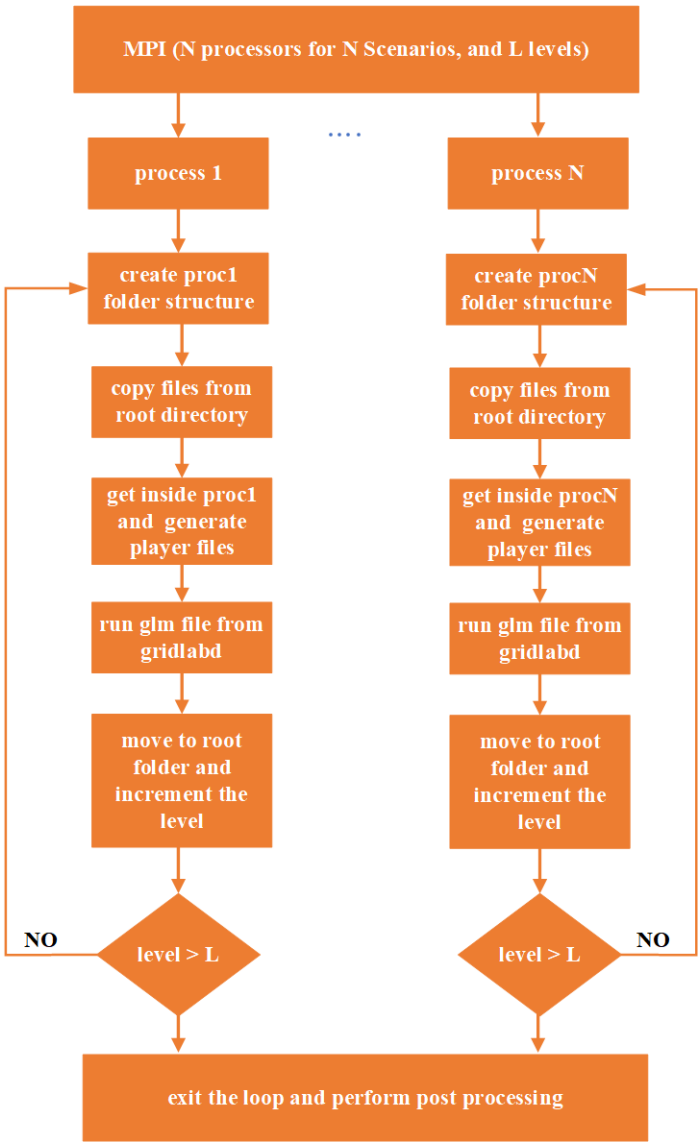

Figure 5.5. Flowchart for splitting hosting capacity analysis in N computer processors.

5.2.5 HPC application

The benefits of using HPC is greater when the size of the problem is relatively large and can be broken into smaller independent pieces with minimal communication. Monte Carlo analysis is a perfect fit for parallel operation as each scenario is independent, i.e., running power flow for each scenario corresponding to each PV penetration level. The large taxonomy feeder network size and small simulation timestep make the use of HPC

even more suited to this problem.

In this study, the PV penetration level is used to indicate the percentage of homes with installed PV, as mentioned before. In this application, 9 different PV penetration levels were identified and shared by 25 different processes. As described in Fig. 5.5, at the outset each process creates a folder structure and copies all required files from the root location. Then, each process generates player input files inside its directory. Each scenario of a particular penetration level is run by a different MPI process, and player files for all 25 scenarios are generated in parallel.

After the generation of all player files for the particular PV penetration level and scenario, a .glm input file is run by GridLAB-D by each process. The .glm file is a population of objects that contains the model of elements of distribution power networks and is used by GridLAB-D to perform power flow (i.e., represents the taxonomy feeder). After performing the power flow for each scenario, each of the processes returns to the root node to start the next penetration level. This loop continues until all power flow is performed for all scenarios. At 100% penetration level, power flow is performed for only one possible scenario. Finally, the results of the power flow for 251 scenarios are exported to be post-processed in MATLAB.

5.2.6 Result analysis

The simulation year was chosen to be 2015, where June 22 correlated to the highest irradiance day, and February 22 was the low load day.

The objectives of this study were two-fold: (i) to distribute each scenario to a specified number of processing elements (in our case we distributed to 25 processors) to

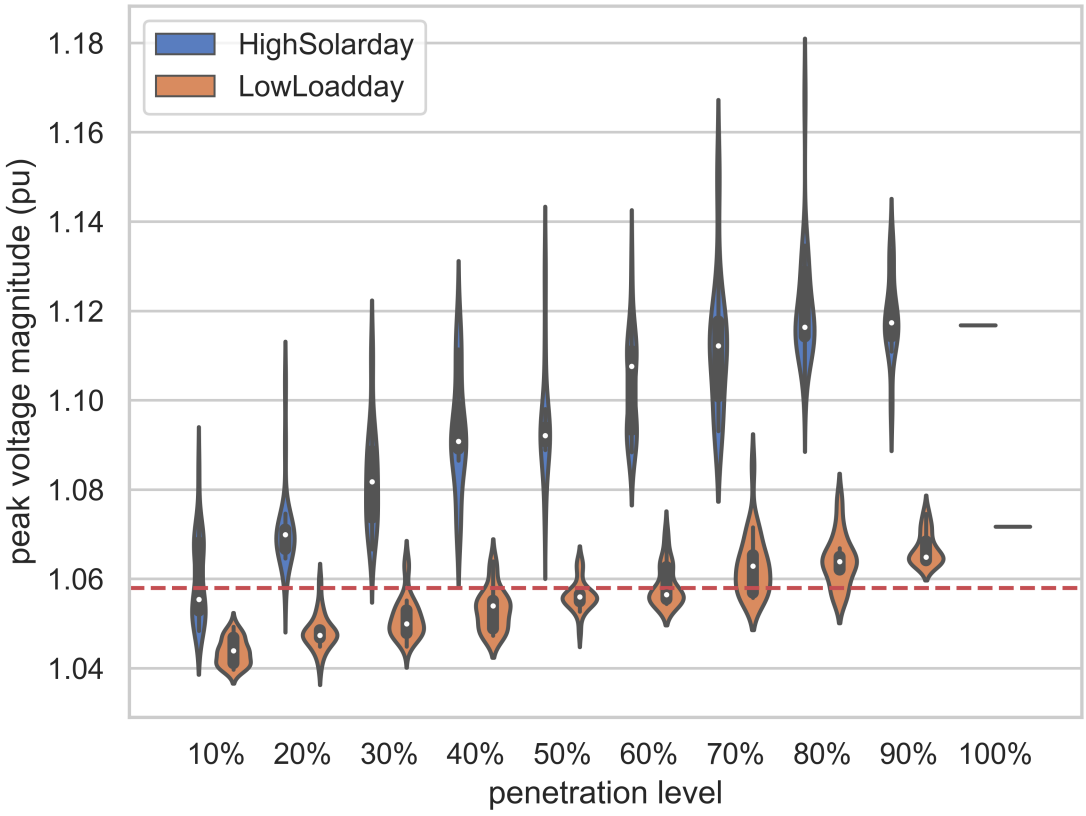

Figure 5.6. Violin plot showing the distribution of maximum voltage magnitudes from all scenarios for each PV penetration level for two different simulation days.

run power flow to obtain voltage magnitudes at each feeder node point under consideration; and (ii) to analyze the voltage measurements to assess the hosting capacity of the feeder. Voltage measurements are used to determine the impact of PV penetration on overvoltage/undervoltage (a situation where the voltage at any node point exceeds the certain upper/lower threshold value) and voltage imbalance between the phases that limit the amount of PV on a distribution grid. In this study, the voltage between 0.95–1.058 p.u. is taken as acceptable voltage ranges defined by the ANSI standard [32].

Figs. 5.6 and 5.7 show the distribution of the minimum and maximum voltage magnitudes collected from all scenarios for each penetration level. For penetration levels

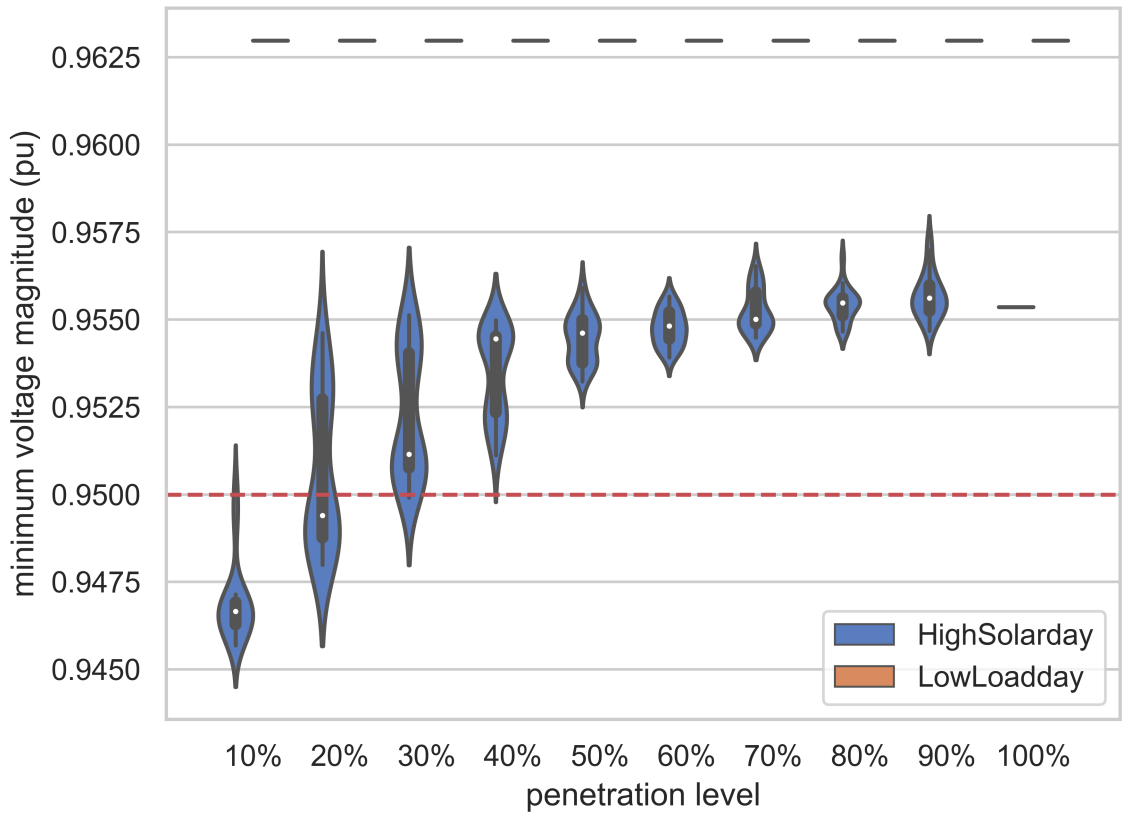

Figure 5.7. Violin plot showing the distribution of minimum voltage magnitudes from all of the scenarios for each PV penetration level for two different simulation days.

up to 30%, the feeder experienced both undervoltage and overvoltage for the highest irradiance day because of peak load shift caused by solar generation. No undervoltage occurs after 30% PV penetration, indicating that the generation coincides with the load pattern. For the low load day, the minimum voltage magnitude was unaffected with variation in penetration level because the peak load occurred during the time when the solar power output is zero for all units.

The observation of peak voltage magnitudes and maximum voltage imbalance (in Fig. 5.8) at 70% and 80% PV penetration level for both simulation days could be due to the random PV allocation in the feeder, causing a large variation in installed PV capacity

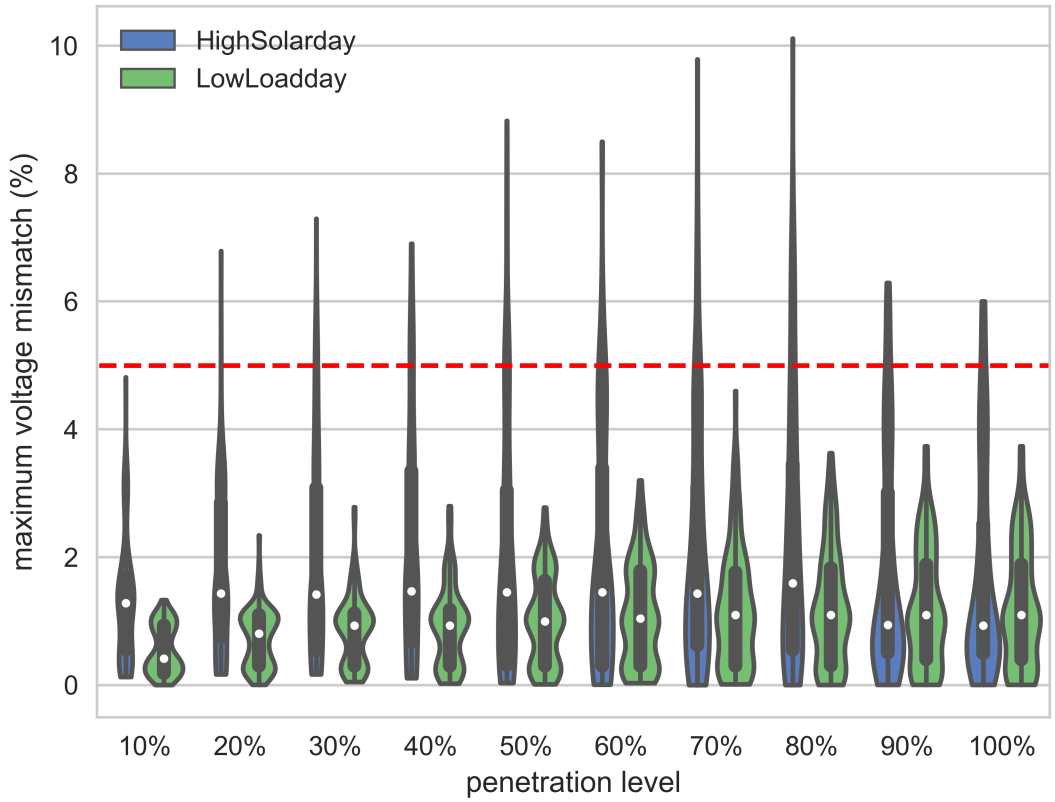

Figure 5.8. Violin plot showing the distribution of maximum percentage voltage mismatch between the phases in each penetration level for two different simulation days.

between the phases.

This mismatch is less than 5% for the 10% and 100% penetration levels because of the relatively symmetrical distribution of PV units in the three phases for both days. The smaller voltage mismatch between phases in the low load day compared to the high irradiance day is because of the lower net generation in the low load day. Fig. 5.9 shows that the number of occurrences of overvoltage (voltage above 1.058 p.u.) increases non-linearly with an increase in penetration level for the high irradiance day. In the low load day, however, overvoltage occurs only after 50% penetration level. Fig. 5.10 shows the distribution of time spent by each processing element to (i) generate the player input

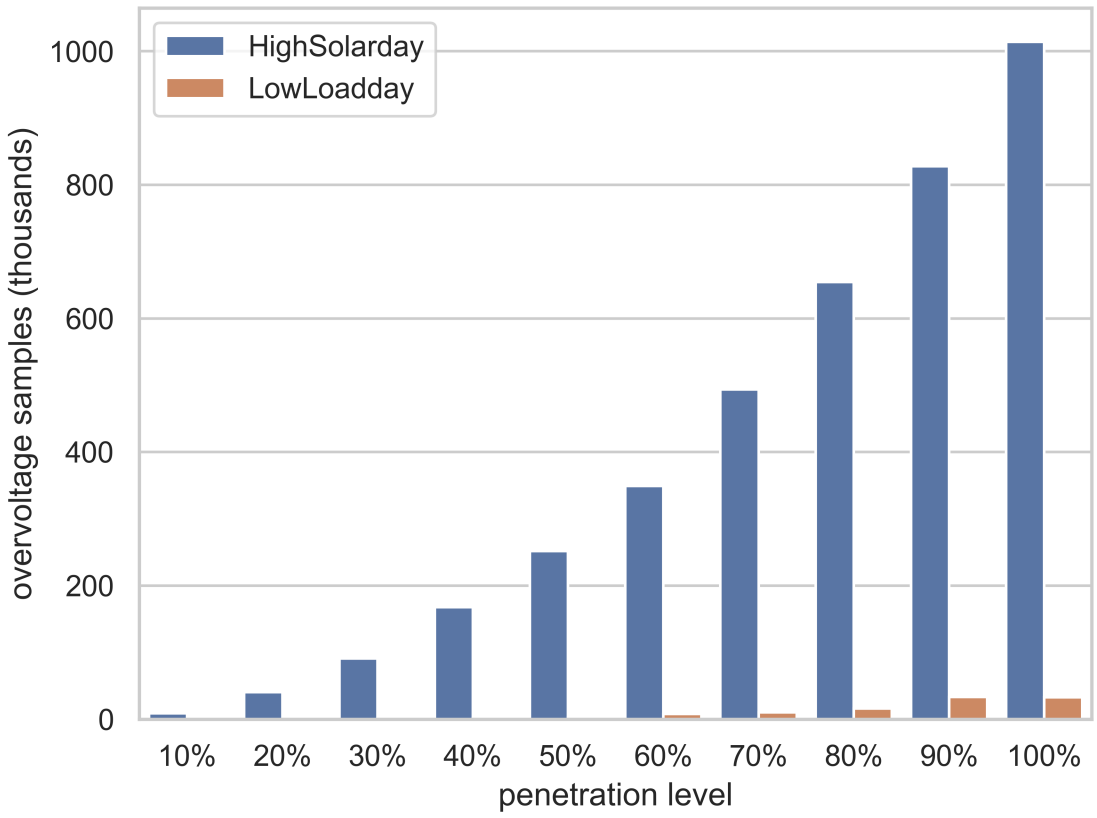

Figure 5.9. Bar graph showing the frequency of overvoltage (voltage above 1.058 p.u.) occurrences for different PV penetration levels for two different simulation days.

files to be used by GridLAB-D, and (ii) run power flow. It is seen that it takes significantly longer to generate the input files than to run power flow. On average, generating a one-day player input file in a one-minute timestep took ∼14 minutes, while running power flow in GridLAB-D only took ∼3.5 minutes. Because each scenario is independent, and each scenario is computationally similar, the execution time did not change as a function of penetration level.

5.2.7 Summary of Study

PV penetration analysis helps to estimate the hosting capacity of a distribution system in giving an estimated amount of PV installation possible before incurring

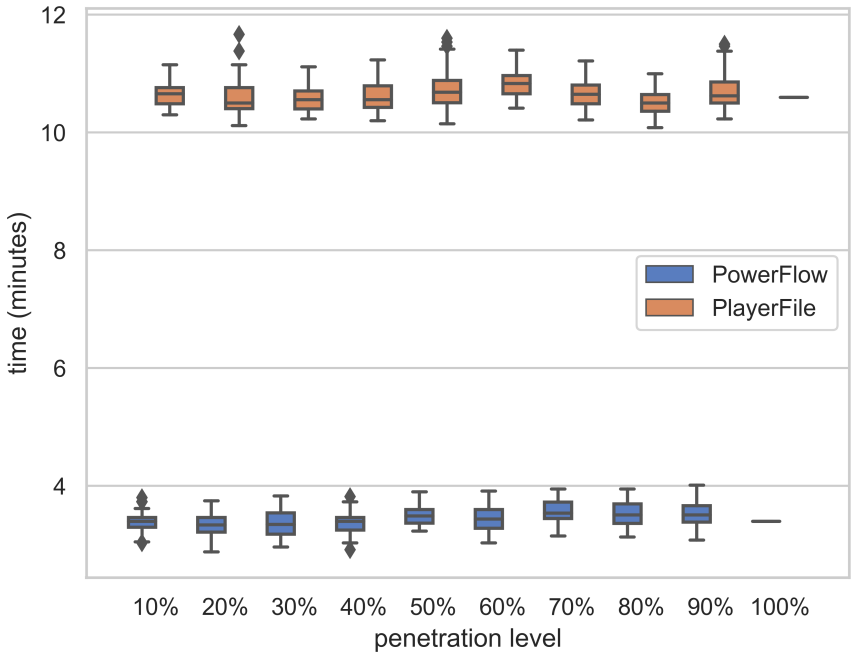

Figure 5.10. Boxplot showing distribution of computation time per processing element at different PV penetration levels for running powerflow and generating player files.

operational issues. Parallel programming models, such as MPI, can be used to split Monte Carlo simulation scenarios among multiple processing elements in an HPC cluster to reduce computation time. In this study, only overvoltage and voltage mismatch between the phases are considered as a reason for limiting hosting capacity of the feeder. For the tested taxonomy feeder, it was found that for the highest annual irradiance day, operational issues occur at only a 10% PV penetration level if no system enhancements are made. For the lowest annual load day, however, the PV hosting capacity was able to operate up to 50% without issue. The developed workflow of HPC-enabled parallel PV hosting capacity Monte Carlo simulation studies can be used by distribution system planners and utility companies to assist in integrating the maximum amount of PV on their system without having technical issues.

CHAPTER 6 CONCLUSIONS

The research work proposed a framework for long-term techno-economic and sustainability assessment of different overvoltage prevention methods using the active and reactive power capabilities of PV inverters along with additional study about the marginal cost of distribution ancillary services, and PV hosting capacity analysis using High-Performance Computing. This framework allows utilities to quantify the techno-economic benefits and sustainability of each method to support their decision-making process in the controller.

In addition, an example study comparing five different PV controller methods was presented. Droop-based APC (LDAPC and QDAPC) inverter controllers were shown to be effective local overvoltage prevention methods that guarantee overvoltages are not caused by PV systems. Using reactive power absorption capability of inverters (such as in ARD and ARPM) reduced the need for active power curtailment. However, the reduction in APC will result in higher transformer and distribution system loading and losses as compared to droop-based APC methods. Coordinating PV inverters reactive power absorption and active power curtailment using communication (e.g., ARPM) reduced the difference in energy generation from PV systems among households and reduced the need of curtailment, although similar performance was shown in the local ARD controller. In feeders with high penetration of PV, the choice of overvoltage prevention method can affect the payback time of customers with PV systems and net revenue earned by utilities.

Implementation of droop-based PV inverter controllers in QSTS (e.g., GridLAB-D) can cause numerical oscillations of the electrical parameter under control, such as voltage.

The proposed network sensitivity-based algorithm eliminated such numerical oscillations. Results showed that the maximum error in converged voltage magnitude was less than 0.5% for all three controllers compared to the dynamic simulation.

Different inverter-based voltage regulation approaches also showed different social, economic, and environmental impacts. Three sustainability metrics were proposed to measure social, economic, and environmental impacts. The use of reactive power to mitigate overvoltage had higher economic, social and environmental benefits. Although the ARPM performed marginally better than ARD, the former may be hard to justify given the increased installation cost from the communication signal and possible cyber-security issues. Optimal inverter control schemes maintaining economic (or environment) and social sustainability were conflicting objectives, and a trade-off became necessary to select optimal inverter setpoints. The trade-off can be used in community PV projects, where PV is pooled as a shared resource to maximize economic/environmental benefits, while the social impact is shared between users. The higher sensitivity of active power to voltage change compared to the reactive power, the locational marginal price for active power curtailment tends to be higher than the locational marginal price for reactive power absorption for PV units located far away from the substation.

Lastly, PV penetration analysis helped to estimate the hosting capacity of a distribution system in giving an estimated amount of PV installation possible before incurring operational issues. Parallel programming models, such as MPI, can be used to split Monte Carlo simulation scenarios among multiple processing elements in an HPC cluster to reduce computation time

Appendix A. Derivation for APC controllers

In this section, $\Delta\mathbf{p}_c^{(k)}$ from (2.6) is derived. Let $\mathbf{v}^{*(k)}$ be a vector of size h which is *estimated* voltage magnitude at each PV inverter given a curtailed power of $\mathbf{p}_c^{(k)}$, given as:

$$\mathbf{v}^{*(k)} = \mathbf{v}^{(k)} - \mathbf{S_p}\Delta\mathbf{p_c}^{(k)}. \tag{A.1}$$

Using the LDAPC relation from (2.1), curtailment for estimated voltage $\mathbf{v}^{*(k)}$ can also be calculated as:

$$\mathbf{p_c}^{(k)} = m_p(\mathbf{v}^{*(k)} - \mathbf{v_{cri}}). \tag{A.2}$$

Merging (2.6) and (A.2), we obtain

$$\mathbf{p_c}^{(k-1)} + \Delta\mathbf{p_c}^{(k)} = m_p(\mathbf{v}^{*(k)} - \mathbf{v_{cri}}). \tag{A.3}$$

Substituting $\mathbf{v}^{*(n)}$ in (A.3), we get:

$$\mathbf{p}_c^{(k-1)} + \Delta\mathbf{p}_c^{(k)} = m_p(\mathbf{v}^{(k)} - \mathbf{S_p}\Delta\mathbf{p}_c^{(k)} - \mathbf{v}_{cri}) \tag{A.4}$$

$$\Delta\mathbf{p_c}^{(k)}(m_p\mathbf{S_p} + \mathbf{I}) = m_p(\mathbf{v}^{(k)} - \mathbf{v_{cri}}) - \mathbf{p_c}^{(k-1)} \tag{A.5}$$

Using the definitions of $\mathbf{B_p}$ and $\mathbf{a_p}$ from Chapter 2,

$$\Delta\mathbf{p_c}^{(k)}\mathbf{B_p} = \mathbf{a_p} \tag{A.6}$$

$$\therefore \Delta \mathbf{p_c}^{(k)} = \mathbf{B_p}^{-1}\mathbf{a_p} \tag{A.7}$$

Similarly, curtailment for QDAPC is calculated using

$$\mathbf{p_c}^{(k)} = s(\mathbf{v}^{*(k)} - \mathbf{v_{cri}})^2. \tag{A.8}$$

Equations (2.6), (A.1), and (A.8) are solved for $\Delta \mathbf{p}_c^{(k)}$.

Appendix B. Derivation for ARD controller

In case of ARD controller, during reactive power absorption mode voltage can be estimated as,

$$\mathbf{v}^{*(k)} = \mathbf{v}^{(k)} - \mathbf{S_q}\Delta \mathbf{q_a}^{(k)}. \tag{B.1}$$

Using the droop reactive relation from (2.3), estimated reactive power absorption can be computed as,

$$\mathbf{q_a}^{(k)} = m_q(\mathbf{v}^{*(k)} - \mathbf{v_{kick}}). \tag{B.2}$$

Merging (2.9) and (B.2), we obtain

$$\mathbf{q_a}^{(k-1)} + \Delta \mathbf{q_a}^{(k)} = m_q(\mathbf{v}^{*(k)} - \mathbf{v_{kick}}). \tag{B.3}$$

The same process can then be used from (A.3)–(A.7) to derive:

$$\Delta \mathbf{q_a}^{(k)} = \mathbf{B_q}^{-1}\mathbf{a_q} \tag{B.4}$$

APC must also be included in voltage estimation when at Q_{max}, written as

$$\mathbf{v}^{*(k)} = \mathbf{v}^{(k)} - \mathbf{S_p}\Delta\mathbf{p_c}^{(k)} - \mathbf{S_q}\mathbf{q_{max}}. \tag{B.5}$$

Following the process from (A.5)–(A.7) and using the definitions of of $\mathbf{B_p}$ and $\mathbf{a_p^*}$ from Chapter 2, we can derive:

$$\Delta\mathbf{p_c}^{(k)} = \mathbf{B_p}^{-1}\mathbf{a_p^*} \tag{B.6}$$

Appendix C. Electric bill

Electric bill for RTP and flat rate tariff are given in table:

Table C.1. Supply Charge

		RTP scheme	Flat rate scheme
Supply charges	Electricity supply charges (per kWh)	*	$0.05865
	Transmission services charge (per kWh)	$0.00844	$0.01122
	Capacity charge (per kW)	$4.69477	-
	Msc procurement component charge (per kWh)	$0.0011	-
* can vary hourly available online **ComEd**			

Table C.2. Delivery Charge

		RTP scheme	Flat rate scheme
Delivery charges	Customer charge	$11.55	$10.53
	Standard metering charge	$4.68	$4.36
	Distribution facilities charge (per kWh)	$0.03484	$0.03156
	Illinois electricity distribution charge (per kWh)	$0.00118	$0.00116

Table C.3. Taxes and Fees

		RTP scheme	Flat rate scheme
Taxes & fees	Environmental cost recovery adj (per kWh)	$0.00026	$0.00038
	Renewable portfolio standard (per kWh)	$0.00094	$0.00189
	Zero emission standard (per kWh)	$0.00196	$0.000195
	Franchise cost (% of delivery charge)	1.92%	2.363%
	Energy efficiency programs (per kWh)	-	$0.00345
	State tax **state˙municipal˙tax** (¢/ kWh)	0.33	0.33
	Municipal tax **state˙municipal˙tax** (¢/ kWh)	0.46	0.46

REFERENCES

[1] Solar Energy Industry Associations, *U.S. Solar Market Insight*, 2018. [Online]. Available: https://www.seia.org/us-solar-market-insight (visited on 10/16/2018).

[2] R. Seguin, J. Woyak, D. Costyk, J. Hambrick, and B. Mather, "High-Penetration PV Integration Handbook for Distribution Engineers," Tech. Rep., 2016, pp. 1–99.

[3] L. Sherwood, *U.S. solar market trends 2013*, July 2014. [Online]. Available: https://irecusa.org.

[4] Energy Information Administration, *Electric Power Monthly*, 2018. [Online]. Available: https://www.eia.gov/electricity/monthly/ (visited on 02/19/2019).

[5] K. A. W. Horowitz, F. Ding, B. Mather, and B. Palmintier, "The Cost of Distribution System Upgrades to Accommodate Increasing Penetrations of Distributed Photovoltaic Systems on Real Feeders in the United States," National Renewable Energy Laboratory, Tech. Rep. NREL/TP-6A20-70710, 2018.

[6] B. Palmintier *et al.*, "On the Path to SunShot: Emerging Issues and Challenges in Integrating Solar with the Distribution System," National Renewable Energy Laboratory, Tech. Rep. NREL/TP-5D00-65331, 2016.

[7] P.-C. Chen, R. Salcedo, Q. Zhu, F. De Leon, D. Czarkowski, Z.-P. Jiang, V. Spitsa, Z. Zabar, and R. E. Uosef, "Analysis of Voltage Profile Problems due to the Penetration of Distributed Generation in Low-Voltage Secondary Distribution Networks," *IEEE Transactions on Power Delivery*, vol. 27, no. 4, pp. 2020–2028, 2012.

[8] R. Tonkoski and L. A. C. Lopes, "Voltage Regulation in Radial Distribution Feeders with High Penetration of Photovoltaic," in *2008 IEEE Energy 2030 Conference*, Nov. 2008, 7 pp.

[9] D. Cheng, B. A. Mather, R. Seguin, J. Hambrick, and R. P. Broadwater, "Photovoltaic (PV) Impact Assessment for Very High Penetration Levels," *IEEE Journal of Photovoltaics*, vol. 6, no. 1, pp. 295–300, Jan. 2016.

[10] J. von Appen, M. Braun, T. Stetz, K. Diwold, and D. Geibel, "Time in the Sun: The Challenge of High PV Penetration in the German Electric Grid," *IEEE Power and Energy Magazine*, vol. 11, no. 2, pp. 55–64, Mar. 2013.

[11] J. M. Guerrero, F. Blaabjerg, T. Zhelev, K. Hemmes, E. Monmasson, S. Jemei, M. P. Comech, R. Granadino, and J. I. Frau, "Distributed Generation: Toward a New Energy Paradigm," *IEEE Industrial Electronics Magazine*, vol. 4, no. 1, pp. 52–64, Mar. 2010.

[12] E. Demirok, D. Sera, R. Teodorescu, P. Rodriguez, and U. Borup, "Clustered PV Inverters in LV networks: An Overview of Impacts and Comparison of Voltage Control Strategies," in *2009 IEEE Electrical Power & Energy Conference (EPEC)*, Oct. 2009, 6 pp.

[13] J. P. Lopes, N. Hatziargyriou, J. Mutale, P. Djapic, and N. Jenkins, "Integrating Distributed Generation into Electric Power Systems: A review of Drivers, Challenges and Opportunities," *Electric Power Systems Research*, vol. 77, no. 9, pp. 1189–1203, July 2007.

[14] R. Tonkoski, L. A. Lopes, and T. H. El-Fouly, "Coordinated active power curtailment of grid connected PV inverters for overvoltage prevention," *IEEE Transactions on Sustainable Energy*, vol. 2, no. 2, pp. 139–147, 2011.

[15] M. E. Elkhatib, R. El-Shatshat, and M. M. A. Salama, "Novel Coordinated Voltage Control for Smart Distribution Networks With DG," *IEEE Transactions on Smart Grid*, vol. 2, no. 4, pp. 598–605, 2011.

[16] O. Homaee, A. Zakariazadeh, and S. Jadid, "Real-time voltage control algorithm with switched capacitors in smart distribution system in presence of renewable generations," *International Journal of Electrical Power & Energy Systems*, vol. 54, pp. 187 –197, 2014.

[17] R. Kabiri, D. G. Holmes, B. P. McGrath, and L. G. Meegahapola, "LV Grid Voltage Regulation Using Transformer Electronic Tap Changing, With PV Inverter Reactive Power Injection," *IEEE Journal of Emerging and Selected Topics in Power Electronics*, vol. 3, no. 4, pp. 1182–1192, 2015.

[18] Y. Wang, P. Zhang, W. Li, W. Xiao, and A. Abdollahi, "Online overvoltage prevention control of photovoltaic generators in microgrids," *IEEE Transactions on Smart Grid*, vol. 3, no. 4, pp. 2071–2078, 2012.

[19] M. Maharjan, "Voltage regulation of low voltage distribution networks," M.S. Thesis, South Dakota State University, 2017, pp. 1–81.

[20] P. Jahangiri and D. C. Aliprantis, "Distributed Volt/VAr control by PV inverters," *IEEE Transactions on Power Systems*, vol. 28, no. 3, pp. 3429–3439, 2013.

[21] J. E. Quiroz, M. J. Reno, O. Lavrova, and R. H. Byrne, "Communication requirements for hierarchical control of volt-var function for steady-state voltage," in *2017 IEEE Power Energy Society Innovative Smart Grid Technologies Conference (ISGT)*, 2017, 5 pp.

[22] F. Olivier, P. Aristidou, D. Ernst, and T. Van Cutsem, "Active Management of Low-Voltage Networks for Mitigating Overvoltages Due to Photovoltaic Units," *IEEE Transactions on Smart Grid*, vol. 7, no. 2, pp. 926–936, 2016, ISSN: 19493053. DOI: 10.1109/TSG.2015.2410171.

[23] R. Tonkoski and L. A. C. Lopes, "Impact of active power curtailment on overvoltage prevention and energy production of PV inverters connected to low voltage residential feeders," *Renewable Energy*, vol. 36, no. 12, pp. 3566–3574, Dec. 2011.

[24] T. Stetz, K. Diwold, M. Kraiczy, D. Geibel, S. Schmidt, and M. Braun, "Techno-economic assessment of voltage control strategies in low voltage grids," *IEEE Transactions on Smart Grid*, vol. 5, no. 4, pp. 2125–2132, 2014.

[25] A. Latif, W. Gawlik, and P. Palensky, "Quantication and Mitigation of Unfairness in Active Power Curtailment of Rooftop Photovoltaic Systems Using Sensitivity Based Coordinated Control," *Energies*, vol. 9, no. 6, pp. 1–16, 2016.

[26] A. I. Nousdilis, G. C. Christoforidis, and G. K. Papagiannis, "Active power management in low voltage networks with high photovoltaics penetration based on prosumers' self-consumption," *Applied Energy*, vol. 229, no. 1, pp. 614 –624, 2018.

[27] M. M.V. M. Ali, P. H. Nguyen, W. L. Kling, A. I. Chrysochos, T. A. Papadopoulos, and G. K. Papagiannis, "Fair power curtailment of distributed renewable energy sources to mitigate overvoltages in low-voltage networks," in *2015 IEEE Eindhoven PowerTech*, 2015, pp. 1–5.

[28] F. Sahriatzadeh, P. Nirbhavane, and A. K. Srivastava, "Locational marginal price for distribution system considering demand response," in *2012 North American Power Symposium (NAPS)*, 2012, 5 pp.

[29] L. Bai, J. Wang, C. Wang, C. Chen, and F. Li, "Distribution locational marginal pricing (dlmp) for congestion management and voltage support," *IEEE Transactions on Power Systems*, vol. 33, no. 4, pp. 4061–4073, 2018.

[30] A. Papavasiliou, "Analysis of distribution locational marginal prices," *IEEE Transactions on Smart Grid*, vol. 9, no. 5, pp. 4872–4882, 2018, ISSN: 1949-3053. DOI: 10.1109/TSG.2017.2673860.

[31] IEEE Std 1547-2003, *IEEE Standard for Interconnecting Distributed Resources with Electric Power Systems*, 2003. DOI: 10.1109/IEEESTD.2003.94285.

[32] ANSI C84.1, *Voltage Rating for Electric Power Systems and Equipment*, 1989.

[33] D. P. Chassin, K. Schneider, and C. Gerkensmeyer, "Gridlab-d: An open-source power systems modeling and simulation environment," in *2008 IEEE/PES Transmission and Distribution Conference and Exposition*, 2008, pp. 1–5.

[34] T. M. Hansen, B. Palmintier, S. Suryanarayanan, A. A. Maciejewski, and H. J. Siegel, "Bus.py: A gridlab-d communication interface for smart distribution grid simulations," in *2015 IEEE Power Energy Society General Meeting*, 2015, pp. 1–5.

[35] T. M. Hansen, E. K. P. Chong, S. Suryanarayanan, A. A. Maciejewski, and H. J. Siegel, "A Partially Observable Markov Decision Process Approach to Residential Home Energy Management," *IEEE Transactions on Smart Grid*, vol. 9, no. 2, pp. 1271–1281, 2018, ISSN: 1949-3053.

[36] SolarAnywhere, *Clean Power Research*, 2017. [Online]. Available: https://www.solaranywhere.com.

[37] SOLAR ELECTRIC SUPPLY, *8.4 KW SolarWorld Sunmodule Plus SW 280 Mono Solar Panel System*, 2017. [Online]. Available: https://www.solarelectricsupply.com/8-4-kw-solaria-powerxt-350r-pd-all-black-solar-panel-system.

[38] ComEd, *Real-Time Hourly Pricing*, 2019. [Online]. Available: https://hourlypricing.comed.com/live-prices/.

[39] R. Fu, D. Feldman, R. Margolis, M. Woodhouse, K. Ardani, R. Fu, D. Feldman, R. Margolis, M. Woodhouse, and K. Ardani, "U.S. Solar Photovoltaic System Cost Benchmark: Q1 2017," Tech. Rep. NREL/TP-6A20-68925, 2017.

[40] United Nations, "Report of the World Commission on Environment and Development: Our Common Future," Tech. Rep. A/42/427, 1987.

[41] J. Carpenter and M. Turró, "Measuring Social Sustainability: Best Practice from Urban Renewal in the EU," *2008/01: EIBURS Working Paper Series*, pp. 1–22, 2008.

[42] Southern California Edison, *Time-of-Use (TOU) Rate Plans*, 2019. [Online]. Available: https://www.sce.com/residential/rates/Time-Of-Use-Residential-Rate-Plans.

[43] PJM, *Real-Time Hourly LMPs*, 2019. [Online]. Available: https://dataminer2.pjm.com/feed/rt_hrl_lmps/definition.

[44] S. V. Dhople, S. S. Guggilam, and Y. C. Chen, "Linear Approximations to AC Power Flow in Rectangular Coordinates," in *Allerton Conference on Communication, Control, and Computing*, 2015, pp. 211–217.

[45] E. Dall'Anese and A. Simonetto, "Optimal Power Flow Pursuit," *IEEE Transactions on Smart Grid*, vol. 9, pp. 942–952, 2018.

[46] K. Deb, *Multi-Objective Optimization Using Evolutionary Algorithms*. John Wiley & Sons, 2011.

[47] A. K. Abu-Rumman, I. Muslih, and M. A. Barghash, "Life Cycle Costing of PV Generation System," *Journal of Applied Research on Industrial Engineering*, vol. 4, no. 4, pp. 252–258, 2017.

[48] R. Fu *et al.*, "U.S. Solar Photovoltaic System Cost Benchmark: Q1 2017," National Renewable Energy Laboratory, Tech. Rep. NREL/TP-6A20-68925, 2017.

[49] K. A. W. Horowitz, F. Ding, B. Mather, and B. Palmintier, "The Cost of Distribution System Upgrades to Accommodate Increasing Penetrations of Distributed Photovoltaic Systems on Real Feeders in the United States," Tech. Rep. NREL/TP-6A20-70710, 2018, pp. 1–35.

[50] J Bank, B Mather, J Keller, and M Coddington, "High Penetration Photovoltaic Case Study Report," Tech. Rep. NREL/TP-5500-54742, 2013, pp. 1–23.

[51] A. Woyte, V. V. Thong, R. Belmans, and J. Nijs, "Voltage Fluctuations on Distribution Level Introduced by Photovoltaic Systems," *IEEE Transactions on Energy Conversion*, vol. 21, no. 1, pp. 202–209, 2006.

[52] G. Amaro-Rico, S. Botello-Rionda, and M. Carrillo-Tripp, "Linear Complexity and High Scalability of a Parallel Monte Carlo Simulation Method," in *International Conference on P2P, Parallel, Grid, Cloud and Internet Computing*, 2013, pp. 683–687.

[53] W. El-Khattam, Y. G. Hegazy, and M. M. Salama, "Investigating Distributed Generation Systems Performance Using Monte Carlo Simulation," *IEEE Transactions on Power Systems*, vol. 21, no. 2, pp. 524–532, 2006.

[54] K. Schneider, D. Engel, Y Chen, S. Thompson, D. Chassin, and R. Pratt, "Modern Grid Initiative Distribution Taxonomy Final Report," Pacific Northwest National Laboratoty, Tech. Rep. PNNL-18035, 2008.

[55] M. A. Cohen, *GridLAB-D Taxonomy Feeder Graphs*, 2018. [Online]. Available: http://emac.berkeley.edu/gridlabd/taxonomy_graphs/.

[56] Energysage, *What is the average solar panel size and weight?* 2018. [Online]. Available: https://news.energysage.com/average-solar-panel-size-weight/.

[57] SolarReviews, *What are the Most Efficient Solar Panels for 2018?* 2018. [Online]. Available: https://www.solarreviews.com/blog/what-are-the-most-efficient-solar-panels-for-2018.

[58] Solar-Estimate, *How many square feet of roof space will I require to install a 6kW solar system?* 2018. [Online]. Available: https://www.solar-estimate.org/solar-panels-101/6kw-solar-system.

[59] California ISO, *Historical hourly load data from EMS*, 2018. [Online]. Available: http://www.caiso.com/planning/Pages/ReliabilityRequirements/Default.aspx#Historical.